



Doctoral Thesis in Material Science

Some aspects of hydrogen reduction of iron ore

OSCAR HESSLING

Some aspects of hydrogen reduction of iron ore

OSCAR HESSLING

Academic Dissertation which, with due permission of the KTH Royal Institute of Technology, is submitted for public defence for the Degree of Doctor of Philosophy on Friday, 12 April 2024, at 09:00 a.m. in D3, Lindstedtsvägen 9, Kungliga Tekniska Högskolan, Stockholm.

Doctoral Thesis in Material Science
KTH Royal Institute of Technology
Stockholm, Sweden 2024

© Oscar Hessling

TRITA-ITM-AVL 2024:5
ISBN 978-91-8040-882-0

Printed by: Universitetservice US-AB, Sweden 2024

Sammanfattning

Reduktion av hematit- och magnetitpulver studerades i ren vätgas i en fluidbädd, i temperaturintervallet 768–888 K. Hematitpellets studerades i en Termogravimetrisk Analysutrustning (TGA), i temperaturintervallet 873–1173 K med en atmosfär av vätgas och 0–15 % $p_{\text{H}_2\text{O}}$. Även termoelement borrades in i kärnan på pellets innan reduktion. Tillsammans med ett termoelement i kontakt med pelletens yta kunde temperaturgradienten i pelleten mätas under reduktionen. Ett alternativt sätt att starta reduktionen i både fluidbädden och TGA-utrustningen användes, där provet introducerades till en varm ugn och en stabil reaktiv atmosfär från ett icke-reagerande tillstånd vid låg temperatur. I den traditionella metoden värms provet upp till den experimentella temperaturen i inert gas, varefter gasen byts ut till en reaktiv gas för att starta reaktionen. Metodförändringen gjordes för att undvika osäkerheter som annars kan introduceras av utspädningssteget i den tidigare metoden. Analys med Sveg Elektron Mikroskopi (SEM) genomfördes för att följa reduktionen.

Båda typerna av malmpulver reducerade med en liknande hastighet. Reduktionen av både pulver och pellets var snabb i början, och hastigheten ökade med en ökande temperatur. Reduktionshastigheten under den sista delen av reduktionen var långsam, och där hade temperaturen inte stor inverkan. För pellets visade ett ökande $p_{\text{H}_2\text{O}}$ värde på sjunkande reaktionshastighet, men effekten avtog med en ökande temperatur. Under reduktionen uppmättes en temperaturskillnad mellan pelletens yta och centrum vid samtliga temperaturer. Ingen skillnad i pelletens makroporositet kunde ses med en ändrad temperatur. Däremot skiljde sig mikrostrukturen i kornen åt. Vid 873 K bildade järnet en porös struktur, men vid en högre temperatur var det bildade järnet solitt. Med ökande $p_{\text{H}_2\text{O}}$ värden vid 873 K sågs pordiametern i järnet öka men antalet porer minska. Porös järnoxid observerades under reduktionen vid samtliga temperaturer och $p_{\text{H}_2\text{O}}$ värden, och ökande temperaturer eller $p_{\text{H}_2\text{O}}$ värden sågs öka pordiametern och minska porantalet. Pelletsegenskaper utvärderades med avseende på sammansättning, genom att tre pelletsammansättningar testades genom ett Cold Crushing Strength (CCS) test, TGA- och smältexperiment. Sammansättningen visade inte på någon förändring med avseende på mekaniska egenskaper eller reduktionsegenskaper, men dess fosforreningssegenskaper varierade med sammansättningen.

Resultaten visar på att reduktionen styrs av flera parallella mekanismer, både vid pulver- och pelletreduktion. Skillnaden mellan den uppmätta temperaturen i provet och den experimentella temperaturen visar en inverkan av både värmetransport och den endotermiska reaktionen. Effekten som $p_{\text{H}_2\text{O}}$ ses ha, visar på inverkan från både diffusion och bakåtreaktionen. Resultaten visar också att den sista delen av reduktionen i huvudsak är styrd av diffusion. Det kunde också visas att pelletens sammansättning kan förändras för att förbättra pelletens användbarhet, utan att påverka dess mekaniska egenskaper eller reduktionsegenskaper.

Abstract

Fines of hematite and magnetite were studied in the fluidized bed using a pure hydrogen atmosphere in the temperature range of 768 to 888 K. Hematite pellets were studied based on Thermogravimetric Analysis (TGA) experiments using hydrogen atmospheres containing 0–15 % $p_{\text{H}_2\text{O}}$, in the temperature range of 873 to 1173 K. Thermocouples in contact with the pellet's surface and embedded in the pellet's center recorded the thermal gradient in the pellet during reduction. The fluidized bed and the TGA experiments used an alternative method to start the reaction. The furnace was pre-heated with a reactive atmosphere. After this, the reaction was initiated by introducing the sample to the hot furnace, to eliminate the effect of gas dilution during gas switching. After the experiments, Scanning Electron Microscopy (SEM) analyses were employed to study the reduction microstructures.

Both types of fines showed similar reduction rates. Fines and pellets showed high initial reduction rates, which increased with increasing temperatures. The reduction rate in the last reduction stage was low for both fines and pellets. An increasing $p_{\text{H}_2\text{O}}$ content in the atmosphere lowered the reaction rate, and the effect decreased with increased temperature. A difference between the pellet's surface and center temperatures was observed during reduction. The pellet's macro-pore structure was seen to be unaltered by changes in temperature or atmosphere. However, at 873 K, the iron product microstructure was found to be highly porous. Furthermore, increasing temperatures caused dense iron to form. In addition, when porous iron or iron oxides were observed, increasing $p_{\text{H}_2\text{O}}$ contents increased the pore diameter but decreased the pore amount. Pellet properties with varied pellet compositions were also investigated using Cold Crushing Strength (CCS), reduction in a TGA setup, and melting experiments. The composition was not found to influence the mechanical or reduction properties but significantly affected the phosphorus refining during melting.

The results showed that a mixed reaction rate control occurred during the early reduction stage for both the fines and the pellets. The temperature differences observed during this reduction stage resulted from a combined effect of heat transfer and an endothermic chemical reaction. The impact of water in the atmosphere influenced the reaction rate through the backward reaction and mass transfer. At 873 K, the retarding effect is mainly caused by the backward reaction. The results show the late stage of reduction to be primarily diffusion-controlled. In addition, it should be possible to alter the pellet composition while maintaining pellet properties to increase the usefulness of the pellet.

Acknowledgements

My research group, past and present members, it never feels like work with you around.

Prof. Du, sure, you are part of the group, but maybe, just sometimes, there might be a tiny feeling of actual work to be done when you are around. Your sharp insights never fail to amaze, be it professionally or privately. I am truly grateful to know you, and to all your support over the years.

Prof. Jönsson, since the first classes during the bachelor, you have always been an inspiration and your enthusiasm really rubs off. Your unwavering trust and support have really helped me through this.

A warm and heartfelt thanks to my family and friends. Without you, your support and good spirits, I would have been seriously lacking in the recuperation and motivation needed to complete this work.

(And yes, this includes you, Du, Johan, Joar, Amanda, Julia and Hedda)

Oscar Hessling, Stockholm, 2024

Supplements

Supplement 1

Experimental study on hydrogen reduction of industrial fines in fluidized bed
Oscar Hessling, Magnus Tottie and Du Sichen
Ironmaking & Steelmaking, 2020, 48:8, 936-943

Supplement 2

The effect of the endothermic reaction nature on the iron ore pellet reduction using hydrogen
Oscar Hessling, Julia Brännberg Fogelström, Niklas Kojola and Du Sichen
Metallurgical and Materials Transactions B, 2022, 53, 1258 - 1268

Supplement 3

The influence of water content on the kinetics and mechanisms of hydrogen reduction using industrial iron ore pellets at 873 K - 1173 K
Oscar Hessling, Julia Brännberg Fogelström, Niklas Kojola and Johan Martinsson

Unpublished work

Supplement 4

Controlling mechanisms during hydrogen reduction of iron ore pellets above 80% reduction degree
Oscar Hessling and Johan Martinsson

Unpublished work

Supplement 5

Effect of CaO/SiO₂ ratio on Phosphorus Distribution in molten H-DRI, and Mechanical Properties and Reducibility of fossil-free iron ore pellets.
Oscar Hessling, Niklas Kojola and Johan Martinsson

Unpublished work

The contributions by the author to the supplements

Supplement 1: Literature survey, built the experimental equipment, all experimental work, most of the writing

Supplement 2: Literature survey, built the experimental equipment, assisted and supervised the experimental work, most of the writing

Supplement 3: Literature survey, built the experimental equipment, all experimental work, most of the writing

Supplement 4: Literature survey, all experimental work, most of the writing

Supplement 5: Literature survey, all experimental except the work conducted at LKAB, most of the writing

Table of Contents

1. Introduction	1
2. Scope of the thesis.....	5
3. Experimental	8
3.1. Materials.....	8
3.2. Setup.....	10
3.2.1. Fluidized bed.....	10
3.2.2. TGA.....	11
3.3. Procedure.....	13
3.3.1. Fluidized bed.....	13
3.3.2. TGA.....	14
3.3.3. Pellet properties.....	15
4. Results	15
4.1. Fluidized bed.....	16
4.2. Pellet microstructure	22
4.3. The effect of the endothermic reaction.....	26
4.4. TGA pellet reduction results	31
4.4.1. The effect of water vapor	31
4.4.2. Late stage reduction	35
4.5. Ore pellet properties	38
5. Discussion	40
5.1. Repeatability and comparison to conventional methods.....	40
5.2. Fluidized bed.....	43
5.3. Pellet reduction.....	45
5.3.1. Mechanism	45
5.3.2. Temperature effect.....	48
5.3.3. Effect of the endothermic reaction	50
5.3.4. Effect of water content in the reaction gas	52

5.4. Pellet properties	55
6. Concluding discussion.....	56
7. Conclusions	60
8. Suggestions for future work	61
9. Sustainability	62
10. References	63

1. Introduction

Iron, or steel, is one of the few commodities omnipresent in our society. There are a few exceptions to the rule: Everything in our modern society uses steel, either built by it or relies upon it in its manufacturing or use. As our society grows, we depend on steel as a stepping stone to further progress. During 2019, the steel industry accounted for 5.5 % of the global energy demand, 15 % of the global coal demand, and 2.5 % of the global natural gas consumption. It produced 2.6 Gt of direct CO₂ emissions and 1.1 Gt of indirect CO₂ emissions, accounting for approximately 11 % of the worldwide CO₂ emissions. In Sweden, the steel industry accounts for roughly 12 % of the total CO₂ emissions, where 7 % originates from the Blast Furnace (BF) operation. [1-3]

The reduction of iron ore is mainly conducted through the BF route. The global iron production in 2022 was 1.3 Gt through the BF route. Today's leading alternative is a natural gas Direct Reduction (DR), produced through a shaft furnace or a fluidized bed. Global iron production in 2022 was 125 Mt through the DR route, of which 0.7 Mt was produced using the fluidized bed. The production of iron through DR has been increasing in recent years to reduce CO₂ emissions, since the BF roughly produces 2 tons of CO₂ per ton of iron, whereas DR roughly produces 1 ton of CO₂ per ton of iron. [1, 4–6] However, the natural gas must be replaced to eliminate the CO₂ emissions from the process. Today's DR processes are operated with a gas composition of approximately 40 % CO and 60 % H₂. A replacement of the last 40 % CO should be possible in similar reactors. Running the DR shaft using natural gas is a well-understood process, but only minor operations with pure hydrogen have been conducted on an industrial scale. Furthermore, unlike the BF process, the DR process does not separate the iron from the gangue elements inherent in the ore. Therefore, to avoid introducing excessive amounts of tramp elements to subsequent process steps, a high iron content is important in the ingoing material, and a high reduction degree is important in the outgoing material.

The fluidized bed is a promising industrial technology, where the iron ore is first ground into particles in the size range of 0.1–2 mm. [7] Thereafter, it is reduced in a bed with a high enough gas flow to suspend individual grains in the gas. The process achieves a large contact area between the oxide and the reducing gas, a short internal transport distance inside the grains, and fast reduction times. It reduces the time spent at elevated temperatures, and a reduction even at low temperatures is rapid. In addition, the process can be operated using magnetite which contains a lower amount of oxygen than

hematite. The amount of hydrogen consumed by the reduction reaction can therefore be lowered. However, implementing the process has proved to be difficult. The Circored process was operated from 1999 to 2005 using pure H_2 , but it has been idle since then. [7] Agglomeration of the particles causes de-fluidization of the bed and is an inherent process problem. The particles tend to stick to each other during the reduction process. [8] The sticking has been linked to the formation of metallic whiskers on the particles. Early research has shown whisker growth to occur when reducing hematite powders in a hydrogen atmosphere. [9] However, the study was conducted in a hydrogen atmosphere of an unknown partial pressure. Later research has shown that the use of pure hydrogen prevents the formation of whiskers. [10] Handling reduced iron oxide fines after reduction is difficult, and bricketing is required to avoid a rapid re-oxidization. The author experienced the difficulties of handling reduced iron powder firsthand: While extracting the first powder sample in the fluidized bed experiments in Supplement 1, the powder re-oxidized violently as it came into contact with air and melted through a plastic sample container.

Today, the predominant process is the shaft furnace DR. A vertical shaft is filled with ore in the form of pellets or lumps and continuously fed with new ore from the top. The reduced product is continuously extracted at the bottom. The reaction gas is introduced at the bottom of the shaft and exits at the top, reducing the burden as it travels upwards. The pellets or lump ore are generally in the size ranges of 9–16 mm and 10–35 mm, respectively. The transport distances in the ore pellets or lumps are longer than in the ore particles used in the fluidized bed. Therefore, the process requires longer reduction times to reach high reduction degrees. The reduction is conducted at a higher temperature than the fluidized bed to speed up the reduction process.

An increase in the reduction temperature increases the reaction rate, as shown in previous research. [11–26] Studies have demonstrated a local minimum of the reaction rate just above the wüstite formation temperature (823 K), and above 1073 K, the reaction rate decreases. [11,12,18] In addition, studies have shown an increasing reaction rate with an increasing hydrogen gas partial pressure if CO, inert gas or H_2O is present. [12–15, 26, 27, 29] The retarding effect of water in the atmosphere has been shown to increase with decreasing temperatures. [26, 28, 30–32] The impact of total system pressure is insignificant in the 1–2 atm range. [16] When diffusion through a product layer is the rate-controlling step, the system pressure has an insignificant effect up to 27 atm. [33]

It has been proposed that the reduction of fines is diffusion-controlled if a solid iron layer has formed on the oxide grains or inside the pores. [32, 34–36] Both the temperature and gas composition have been shown to influence the product morphology. [10, 34, 37, 38] Microstructures formed during the reduction of wüstite fines in H_2/H_2O atmospheres in the temperature span 1073–1173 K were classified into porous iron, porous wüstite covered by dense iron and dense wüstite covered by dense iron. [37] Varying p_{H_2}/p_{H_2O} ratios when reducing magnetite fines above 843 K showed that if p_{H_2} was high, an intermediate layer of wüstite was formed on the magnetite grain, on top of which porous iron was formed; if the p_{H_2} value was low, an intermediate layer of wüstite containing tunnels was formed, while solid iron nucleated on the tunnel walls. It is proposed that a solid layer is always formed initially during reduction in both CO/CO_2 and H_2/H_2O atmospheres but that this layer is broken to form a porous structure when p_{H_2} or p_{CO} values are high. [34, 38] The pore diameter in the porous product decreases in size with a decreasing temperature or an increased gas reduction potential. [34]

Sintering of the product layer does not significantly influence the reduction of hematite powder in a natural gas atmosphere and has been shown to occur mainly after the majority of reduction has occurred. [25, 39] However, hematite reduced to magnetite and annealed, and subsequently reduced to iron in a pure hydrogen atmosphere, reduced slower than the hematite reduced directly to iron in both natural gas and hydrogen. [25, 38]

The reported value of activation energy for the reduction reaction differs by approximately one order of magnitude between sources in the literature (40–120 kJ). [40, 41] This is most likely caused by the multiple controlling mechanisms of the reduction reaction and different laboratories' different experimental setups. Therefore, experimental conditions will vary between laboratories, whereby different controlling mechanisms are investigated, resulting in different activation energies being reported.

Investigations on pellet reduction have proposed several reduction propagation modes. Nucleation and growth have been identified to take place at low temperatures. [17, 18] Layer-by-layer reduction in a topochemical manner has been observed in dense pellets and natural ores. [16–19] A propagating reaction zone containing intermixed phases has been observed in more porous pellets. [12, 22] Nucleation, gas diffusion, and the chemical reaction, or a mix thereof, have been identified as the rate-controlling mechanisms. Heat transfer has also been recognized as a potential rate-limiting mechanism. Thermocouples

embedded in the core of pellets and cylinders have shown significant drops in the core temperature during reduction by hydrogen gas. [33, 42]

When investigating the microstructure of pellets, before and during reduction, the observed pores can be classified into macro- and micro-pores. Macro-pores are formed during pelletizing and are observable as gaps between grains. The macro-pore structure has been shown to coarsen with increasing temperatures and reaction times. [43, 44] Micro-pores are formed during reduction and are observable inside grains. The micro-pores formed in the iron oxide grains were shown to decrease in number and increase in diameter with increasing $p_{\text{H}_2\text{O}}$ content. This was investigated by reducing dense magnetite samples in a hydrogen gas atmosphere containing 0–38 % $p_{\text{H}_2\text{O}}$ in the temperature range of 723 to 1373 K. [34, 45]

To the author's knowledge, a comparison of reductions of hematite and magnetite fines has not been conducted. [25, 35, 39] It has been shown that even different hematite ores reduce with different rates when being compared. [35]

It has been a common practice in fluidized bed experiments to heat the powders to the experimental temperature while being fluidized in inert atmospheres; a switch from inert to reacting gas starts the reduction. [9, 10, 25,39] The effect of the gas switching introduces uncertainties in the gas composition during the initial reduction. Considering the rapid reduction rate, this can correspond to a substantial portion of the total reduction. Similarly, switching an inert gas to a reacting gas at the experimental temperature is commonly used for pellet reduction using a TGA setup. The sample is placed in an inert atmosphere and heated to the experimental temperature, after which the reacting gas is introduced. The gas switching causes an uncertainty in the gas composition during the initial reduction. Therefore, the results obtained from the initial part of the fluidized bed or TGA experiments could be somewhat misleading. This uncertainty would increase as the reaction chamber is increased in size because the inert gas dilution will take a longer time. Therefore, an alternative experimental design is used to eliminate the effect of the gas-switching step and the potential impact of a prior heat treatment. This experimental method is also relevant to studies with water introduced to the atmosphere, where the diluting step will be further enhanced in the gas mixer.

Previous studies on the pellet core temperature have utilized lab-made cylinders or pellets roughly 3 cm in diameter. [33,42] However, industrial

pellets should also be investigated to see if the temperature drop in the sample center persists in smaller samples.

A fundamental understanding of the controlling mechanisms of hydrogen reduction of iron ore is needed to aid the development of the hydrogen reduction process. For this, a precise control of the initial experimental conditions must be known to enable an accurate description of the reduction progression.

The DR process is generally followed by the Electric Arc Furnace (EAF) process, which melts the material and makes some initial refining of the iron, mainly with respect to phosphorus. Reaching high reduction degrees is essential to achieve a high utilization of the mined ore, and a low slag amount and energy consumption upon melting in the EAF. The subsequent phosphorus refining in the EAF is benefitted from a high CaO/SiO₂ ratio. [46–48] Studies have shown reduced iron oxide powders or natural hematite ore fines mixed with slag formers to form an autogenous slag capable of achieving a good phosphorus refining upon melting. [49–52] However, CaO/SiO₂ ratio variations have also been shown to influence pellet mechanical properties. [52–58] In addition, increasing the CaO or SiO₂ contents in the pellet are reported to decrease the reaction rate due to a hindered gas pore diffusion. [59] CaCO₃ has been shown to positively affect the reducing properties due to an increasing pellet porosity as CaCO₃ decomposes. [57,58] Therefore, for a modified pellet to be useful, its mechanical and reducing properties must be determined.

2. Scope of the thesis

The thesis investigates some basic fundamental aspects of iron ore reduction by hydrogen, both in fines, as used in a fluidized bed process, and pellets, as used in a DR shaft process. To bring the research closer to the industrial practice, industrially available oxide fines and oxide pellets are primarily employed in the thesis. In the case of pellets, the effect of the endothermic nature of the reaction, and the impact of water in the hydrogen atmosphere on the reduction will be studied. These effects will be discussed in light of reduction mechanisms under different experimental conditions. In the case of the pellet reduction, the importance of diffusion in the latest reduction stage is also studied. Since the ore pellet should have good properties, alternative pellet compositions are also investigated. In the case of fines, the focus is on the difference in the reduction behaviors of hematite and magnetite ores.

Considering the possible drawbacks of the traditional experimental setups, viz., the fluidized bed and TGA, the thesis employs alternative setups to eliminate the effect of the gas switching and any potential pre-reduction heat treatment of the samples. Eliminating these uncertainties should provide a better understanding of the reaction mechanisms involved in the hydrogen reduction of iron ore, both with respect to fines and pellets.

The thesis is composed of 5 supplements. Supplement 1 investigates the difference between the reduction of hematite and magnetite ore fines in the fluidized bed. This is achieved using a fluidized bed setup and reducing hematite and magnetite ore fines in a pure hydrogen atmosphere. Two temperatures are investigated, and the temperature in the bed is recorded. The changes in microstructure are explored using Scanning Electron Microscopy (SEM) to reveal the reduction mechanism.

Supplement 2 investigates the influence of the endothermic reaction and the reduction progression in a pellet in a pure hydrogen atmosphere in the 873–1173 K temperature interval. The effect of the endothermic reaction is studied by reducing single pellets in a TGA setup, with one thermocouple in contact with the pellet's surface and another embedded in its center. Some samples are quenched at a 20 % reduction degree and investigated using the SEM. The study is expected to reveal the endothermic reaction's significant impact on the reduction rate.

Supplement 3 investigates the effect of the gas composition on the reduction mechanisms and reduction progression in the temperature interval of 873–1173 K. Single pellets are reduced in the TGA setup in a flowing gas with different $p_{\text{H}_2}/p_{\text{H}_2\text{O}}$ ratios and temperatures. SEM investigations are conducted on samples quenched at 50 % reduction degree to gain insights into the reaction mechanisms and the effect of the presence of water on the reduction.

Supplement 4 investigates the late reduction stage, >80 % reduction degree, where mass transfer begins to dominate. Single pellets are reduced in the TGA setup at 1123 K to 80, 85, or 90 % reduction degrees. Thereafter, the temperature is lowered to 923, 973, or 1023 K. This study is expected to reveal the importance of diffusion in the later reduction stage. For a better understanding, samples are also investigated using SEM.

Supplement 5 studies the effect of pellet composition on the pellet's properties. Pellets of different compositions are employed to examine the impact of

composition on the reducibility, Cold Crushing Strength (CCS), and the capacities of the autogenous slag on dephosphorization.

In Figure 1, the supplements are presented graphically, and how they relate to the thesis goal. The main focus is on the pellet, as previously stated, and this emphasis is clearly shown in the figure. In addition, insights gained from the reduction of ore fines give some understanding of the reduction mechanisms of the ore pellet.

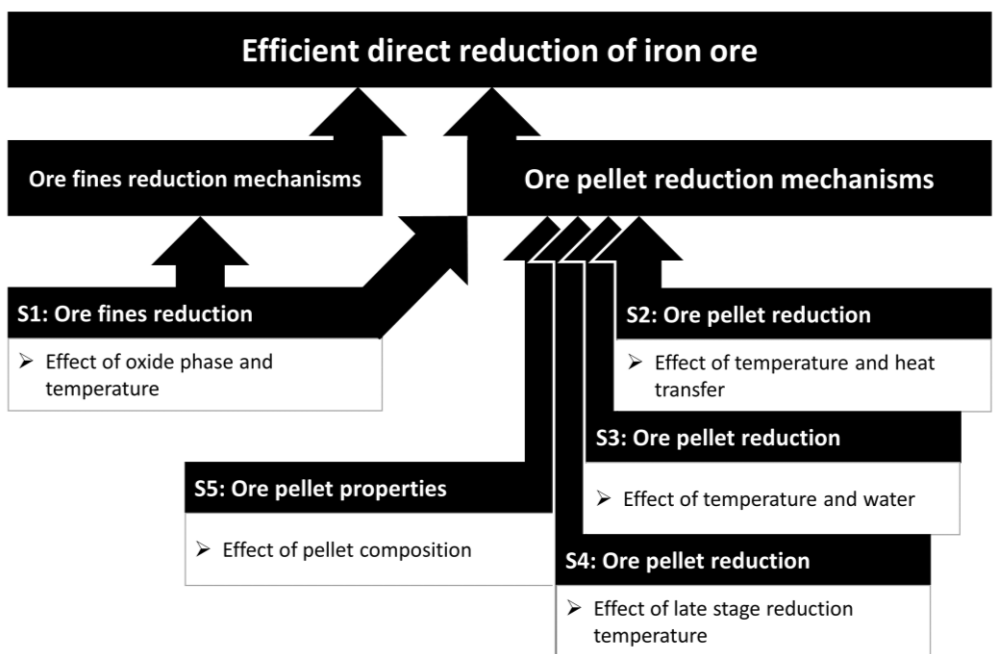


Figure 1 Structure of supplements

3. Experimental

This work utilized two non-conventional experimental setups: namely, a fluidized bed and a TGA unit. While the experimental methods had previously been developed in the laboratory by the research group, the author built the presently used setups. It should be pointed out that both mass transfer and heat transfer play important roles in the reactors of the process. On the other hand, the convection in an industrial process is always a property of the specific reactor. Hence, these studies did not focus on the effects of mass transfer or heat transfer by convection in the bulk of the gas phase. For this purpose, a high enough gas flow rate was employed to ensure that at and above this gas flow rate, the mass and heat transfers in the bulk of the gas did not affect the reduction results.

3.1. Materials

In the fluidized bed study, Supplement 1, two powders were studied: one magnetite powder and one hematite powder (with approximately 9 % magnetite). Their compositions are given in Table 1.

Table 1 Composition and size fraction of the two powders used in the experiments.

[wt. %]	Magnetite	Hematite
Fe	70.5	67.6
O	27.1	29.1
Other oxides	2.1	3.4
Size fraction		
>0.5 mm	51.5	50.1
<0.2 mm	18.7	5.1

The material used for the TGA studies, in Supplements 2–4, was the industrial LKAB KPRS hematite ore pellet supplied by LKAB. Pellets with a weight of $3.5 \text{ g} \pm 0.05 \text{ g}$ and better spherical shapes were selected for the experiments to ease the comparison of the results. However, the sphericity was never perfect, as is the case with industrial pellets. Therefore, no attempt was made to sort the pellets based on the diameter.

For the pellet properties study, Supplement 5, LKAB supplied three types of pellets with varying compositions. The pelletizing process will not be presented due to the interest of the supplier. However, Pellet 2 was produced

with the same composition as the KPRS pellet and represented the commercial reference. The two additional pellets were varied in their CaO/SiO₂ ratios around the reference composition: one below, at 0.8, and one above, at 1.4. To further broaden the CaO/SiO₂ range of the study, two compositions were mixed in the lab and tested in the form of discs, one at a 0.3 and one at a 2.4 CaO/SiO₂ ratio. All compositions are listed in Table 2.

Table 2 Disc and pellet compositions, in an ascending order with respect to the CaO/SiO₂ ratio. Pellet 2 was produced with a commercial reference composition.

[wt. %]	Disc 1	Pellet 1	Pellet 2	Pellet 3	Disc 2
Fe	70.96	67.73	67.78	67.73	67.52
P ₂ O ₅	0.07	0.06	0.06	0.06	0.06
SiO ₂	0.81	1.05	0.82	0.84	0.77
CaO	0.25	0.85	0.97	1.16	1.85
Tot. non-ferrous oxides	1.85	3.14	3.45	3.19	3.44
CaO/SiO ₂	0.31	0.81	1.19	1.39	2.40

The hydrogen and argon gases used for all experiments had a purity of 99.995 % and 99.999 %, respectively.

3.2. Setup

3.2.1. Fluidized bed

The setup used for fluidized bed experiments in Supplement 1 is described in Figure 2.

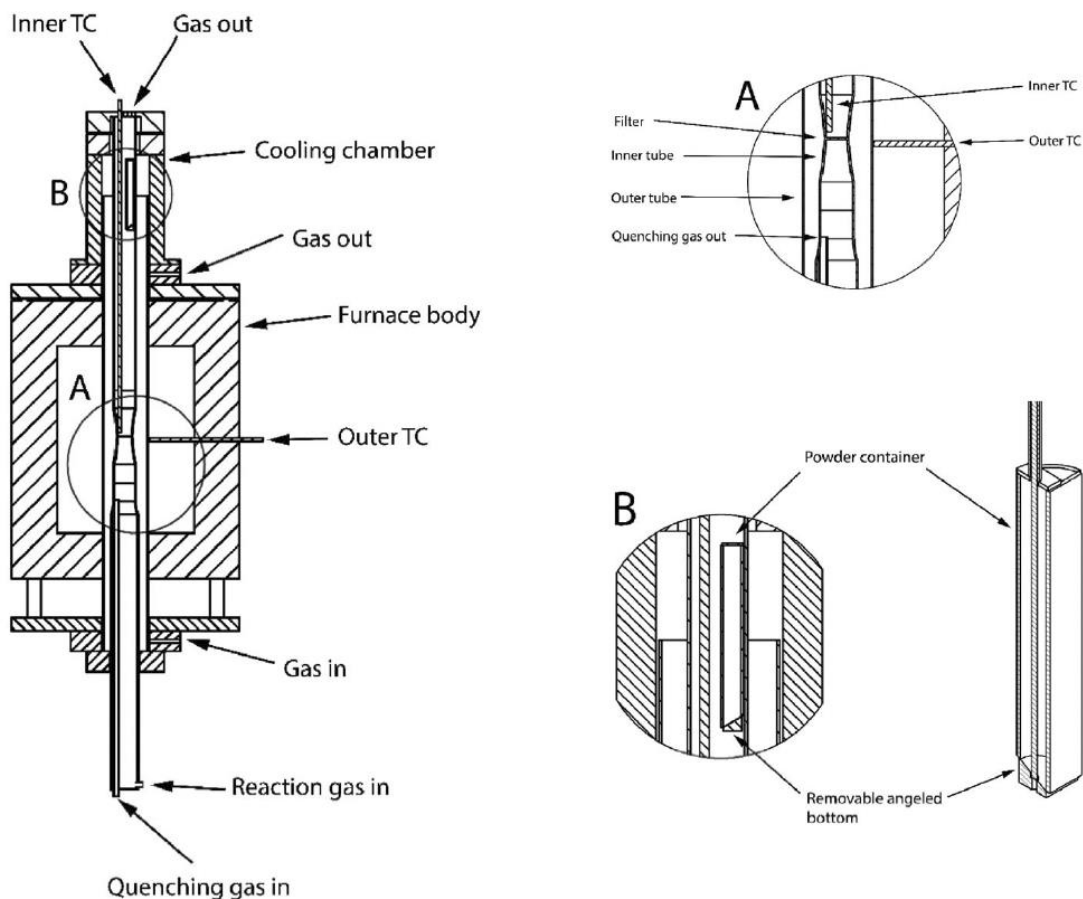


Figure 2 A schematic illustration of the fluidized bed setup.

A resistance-heated vertical tube furnace was employed. The furnace was fitted with two concentric quartz tubes. Outside the outer tube, a type-S thermocouple was placed in the hot zone to control the furnace temperature. The outer tube (90 mm ID) was filled with argon gas for safety reasons. The inner tube (40 mm ID) was made narrow in the furnace hot zone (30 mm ID) and fitted with a quartz filter. The fluidization of the powder bed was achieved

above the filter. Above the filter, not in contact with the wall, a type-K thermocouple was placed to monitor the temperature in the bed. A powder container was positioned further up the inner tube, where the temperature was lower (low enough to avoid any reduction). The container had an open top and removable bottom. Iron oxide powder was placed inside the container. By removing the bottom of the container, the powder was dropped onto the filter to start the experiment. Below the filter, the inner tube was filled with quartz raschig rings to preheat the reaction gas. A narrow tube was passed through the raschig rings to allow the quenching gas to pass through the lower part of the furnace with a minimal heating. The system was sealed vacuum-tight by water-cooled aluminum caps on the ends of both inner and outer tubes.

3.2.2. TGA

A vertical resistance-heated furnace was employed for the TGA experiments in Supplements 2–5. The constant temperature zone was 100 cm long. The setup is illustrated in Figure 3. For a more thorough description, please see Supplements 2–5.

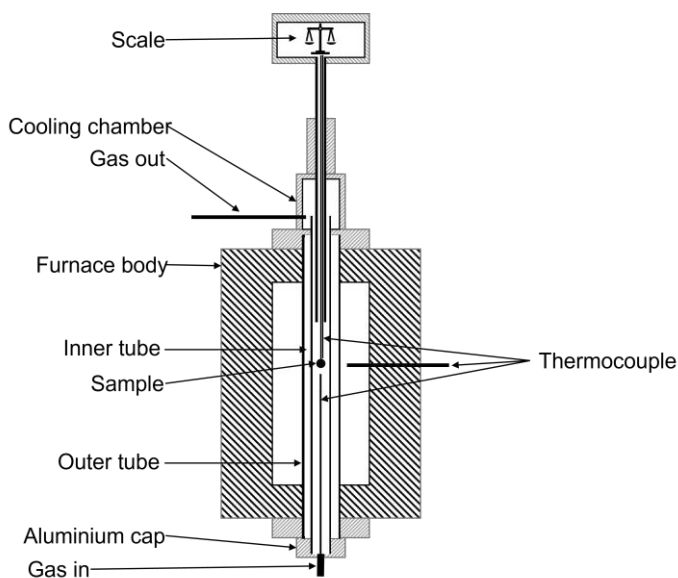


Figure 3 A schematic illustration of the TGA setup.

The furnace was equipped with two concentric quartz tubes (ID 92 mm and 40 mm, respectively) and a type-S thermocouple for the furnace temperature control. In the furnace hot zone, inside the inner tube, a type-K thermocouple

was mounted. The furnace was sealed vacuum-tight with water-cooled O-rings and aluminum caps. The top of the furnace was equipped with a water-cooled sample cooling chamber. Above the cooling chamber, a scale was mounted on a linear motion system, allowing for a vertical movement of the scale. The samples were hung from below the scale in a basket made of nichrothal wire. Another type-K thermocouple was placed in close proximity to the sample, which followed the movement of the sample, to monitor the temperature at the sample position continuously. Gas entered the furnace at the bottom inlet and exited at the top through the cooling chamber. The gas flow was controlled by Bronkhorst el-select mass flow meters.

In the study of the influence of water on reduction (Supplement 3), water was introduced to the gas through a specifically designed water bath. A precise control of the water partial pressure in the gas phase was essential for the experiments investigating the effect of H₂O content on the reduction. A 200 liter insulated water bath was connected to the furnace, with a 30 m (26 mm inner diameter) copper pipe submerged in the liquid, as illustrated in Figure 4.

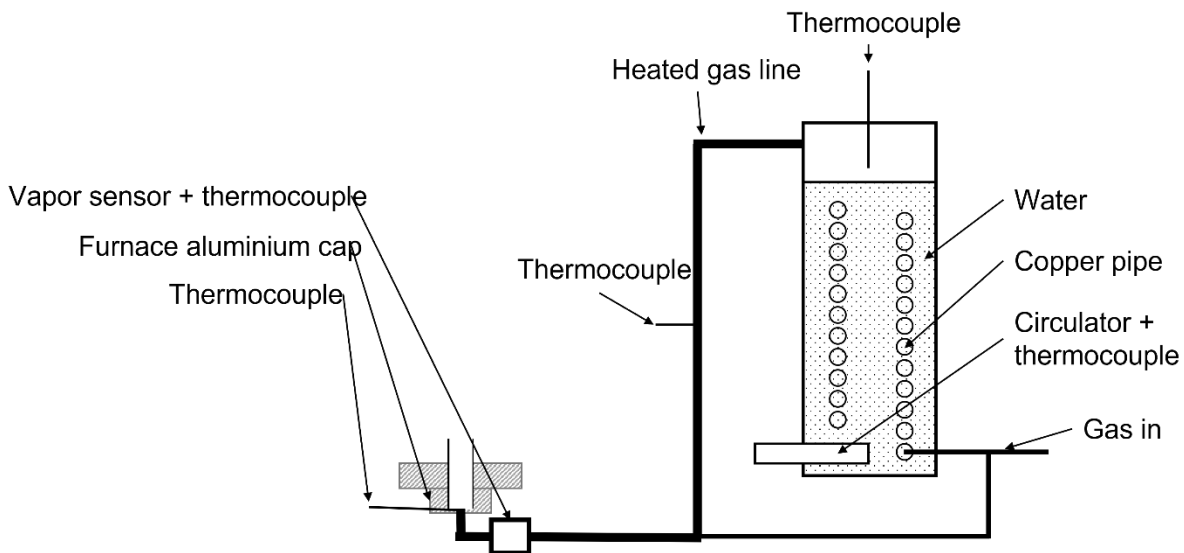


Figure 4 The water vapor partial pressure control unit, a schematic illustration.

A 2000 W circulator with a ± 0.5 K accuracy was employed for temperature control, and the gas line to the furnace was heated. The temperature was recorded in the water, above the water surface inside the chamber, on the outside of the heated gas line, in the gas stream just before the furnace, and in

the wall of the furnace where the gas passed through the water-cooled cap. The furnace was also equipped with a water vapor sensor, placed at the furnace inlet, which continuously monitored the partial pressure of water in the ingoing gas stream.

Passing the gas through a water bath and setting the partial pressure of water with the bath temperature was considered to be the most robust way to ensure the homogeneity of the gas phase. A long enough underwater travel time was needed to ensure the gas is properly heated and achieve thermodynamic equilibrium. A large enough volume of water was necessary to store enough heat in the bath to keep the temperature constant, even if a cold reaction gas was introduced.

Care also had to be taken inside the furnace. For this purpose, the furnace was equipped with clear quartz tubes to inspect the sample and reaction chamber visually. All surfaces the water-containing gas would come in contact with before it passed the sample had to be adequately heated. Type-K thermocouples were inserted into the walls of the lower water-cooled aluminum parts. The top part of the furnace was redesigned so that no water would condense inside the inner tube nor drip into the reaction chamber from any surface. The resting position of the sample in the top part of the furnace was kept at 393 K.

3.3. Procedure

3.3.1. Fluidized bed

In Supplement 1, 14 g of powder was used for each experiment, and a hydrogen gas flow of 31 nl/min was used to fluidize the powder. The furnace was preheated to a temperature above the experimental temperature under an argon gas flow of 0.5 nl/min. When the furnace reached the target temperature, the experimental gas flow was introduced to the furnace. The high flow was associated with a temperature drop in the hot zone, and the gas needed to flow continuously for 30 minutes for the furnace to stabilize at the experimental temperature. The prolonged flushing also allowed for the chamber atmosphere to stabilize. The powder was released and fluidization initiated when the reaction chamber was ready. Fluidization in the reaction gas was allowed for a set amount of time. The reaction gas was replaced with argon at a fluidization flow to stop the reaction. The furnace was cooled to room temperature at approximately 10 K/min. Under constant argon protection, samples were removed from the chamber into argon-filled bottles. The sample structure was investigated by using SEM. Samples were also sent for oxygen content

determination using a Leco-ONH instrument; where the error margin was ± 10 % of the measured value.

3.3.2. TGA

For the TGA studies in Supplements 2–5, a single iron ore pellet was placed in the furnace cold zone, and the furnace was sealed. The furnace atmosphere was set by evacuating the furnace with a vacuum pump down to a pressure of 0.2 bar, after which it was refilled with hydrogen. This procedure was repeated three times. When the atmosphere had been replaced, the furnace was heated to the experimental temperature. After that, the sample was lowered from the furnace cooling chamber into the hot zone to start the experiment. The sample was rapidly moved back to the cold zone when the experiment was finished. During the experiment, the sample weight was recorded continuously. After the experiment, the pellets were immediately weighed and cast in epoxy. Thereafter, the sample structure was investigated by using SEM.

For the study of the late stage of reduction, Supplement 4, an additional type-K thermocouple was placed at the second resting position of the sample. The furnace was heated to the experimental temperature, and the sample was introduced to the furnace hot zone. When the sample had lost the mass corresponding to a specific reduction degree, determined by its initial mass, it was moved to the lower-temperature position. There, it was reduced for an additional 20 min and then transferred to the cooling chamber.

The heat transfer investigation in Supplement 2 was conducted with the addition of two type-S thermocouples having a diameter of 1.1 mm. A 1.2 mm diamond-coated drill was employed to drill one hole to the center of the pellet. One thermocouple was inserted into the pellet, and the other was placed in contact with the pellet surface, as illustrated in Figure 5.

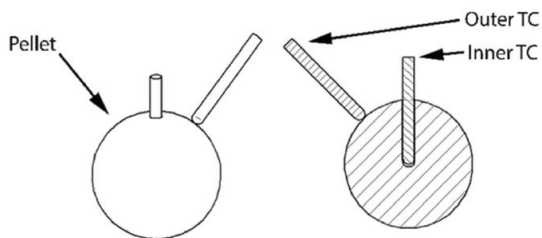


Figure 5 Thermocouple placements.

The experiments conducted with a hydrogen and water mixture in Supplement 3 required some preparation of the water vapor generator. A 15 cm gap was allowed between the water bath surface and the top of the reactor to avoid water droplets in the gas phase. However, the gas in this space had to be hydrogen. Therefore, to remove the air, the water level was increased to remove the gap. After that, hydrogen was introduced to the chamber, and the water level was lowered to the appropriate height. The process was repeated three times to ensure a pure hydrogen/water mixture above the surface. The bath was heated to the desired temperature, and any overpressure was released. After that, the system was sealed and left to equilibrate overnight. The generator was opened to the furnace before the experiment when the gas line and all relevant parts of the furnace were heated above the gas's dew point. Hydrogen was allowed to flow through the water bath into the furnace at the experimental gas flow. The water partial pressure in the flowing gas stream was calibrated by adjusting the water bath temperature according to the online vapor sensor at the furnace inlet. When the appropriate gas composition was reached, the gas mixture was allowed to flow through the furnace at experimental flow rates for at least 30 minutes before the start of the experiment.

3.3.3. Pellet properties

In Supplement 5, the Cold Compressive Strength of the pellets was tested according to ISO 4700, conducted by LKAB. In addition, the reducibility was tested using the TGA setup. Dephosphorization properties were tested according to the method employed by Huss et al. and Vickerfält et al. [50–51] Pellets of each composition were reduced in a pellet bed to a reduction degree of 97.5 ± 0.5 . After that, 100 g of the reduced material was put in a magnesia crucible equipped with a close-fitting molybdenum lid and molten under an argon atmosphere at 1873 K. The time to melt the sample at the temperature in the experimental setup was estimated to be 18 min. The sample was kept in the furnace hot zone for 20 minutes to ensure that it was fully molten. [50]

4. Results

To discuss the results obtained from the reduction experiments, the reduction degree is defined in eq. (1),

$$R \% = \left(1 - \frac{W_{O,t}}{W_{O,0}}\right) * 100 \quad (1)$$

where $W_{O,0}$ is the calculated mass of oxygen bound to iron before reduction, as obtained from the pellet analysis; $W_{O,t}$ is the amount of oxygen bound to

iron in the sample at time t , as calculated from the scale data. Previous investigations have shown that only ferrous oxides are reduced under the experimental conditions. [51] Therefore, all sample weight loss is assumed to originate from this reaction. After reducing the powders, the oxygen content was determined using a LECO-O instrument.

4.1. Fluidized bed

Results from the fluidized bed experiments show the reduction of fines to be initially rapid but significantly slowed down as the reduction progresses. Figure 6 shows the reduction progression of magnetite powder at three different temperatures. After 120 s, the powder has reached 34 and 73 % reduction degrees at temperatures of 768 and 888 K, respectively, showing an initially increasing reaction rate with an increasing temperature. At 768 K, the reduction degree rises from 63 to 89 % in the 600 to 900 s timespan. In the same time period, but at 838 and 888 K, their respective reduction degrees increase from 87 to 88 % and from 91 to 96 %. The reduction rate in the 600–900 s interval is higher at 768 K compared to 838 and 888 K. At higher temperatures, the trend of reduction degree over time is clearly slowed above 80 %. In addition, the powder requires a substantial amount of time to reduce entirely in all temperatures (>900 s).

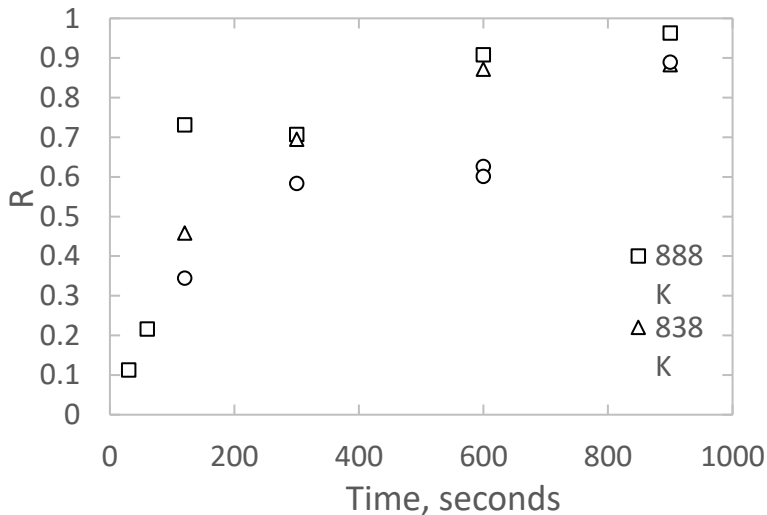


Figure 6 Reduction degree of magnetite powder at temperatures of 768, 838, and 888 K.

Figure 7 shows the reduction of the hematite powder over time. After 120 s, the powder has reached 19 and 82 % reduction degrees at temperatures of 768 and 888 K, respectively. Increasing temperatures are seen to increase the initial reaction rate. In the timespan of 600 to 900 s, the reduction degree rises from 78 to 86 % and from 94 to 95 % at 768 and 888 K, respectively. The trend of an increasing reduction degree over time is significantly slowed in the 600–900 s interval compared to the 0–120 s interval. The trend in Figure 7 shows a fast initial reduction and a significant slowing of reaction during the later stage of reduction, the same trend was seen in the magnetite reduction experiments at 838 and 888 K.

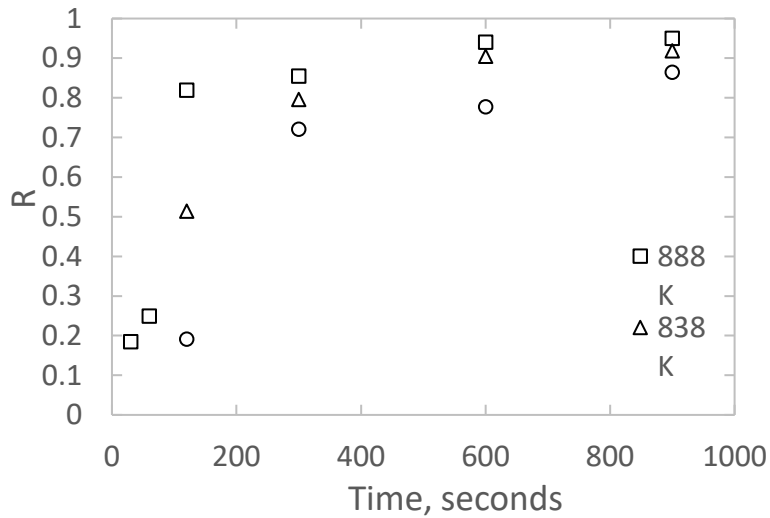


Figure 7 Reduction degree of hematite powder, at temperatures of 768, 838, and 888 K.

SEM investigations were conducted on both powders to investigate the reduction progress and compare the two oxides. Micrographs of both powders after 30, 60, 120, and 600 s reductions at a temperature of 888 K are shown in Figure 8 and Figure 9. The growth of a product layer on the grain surface can be observed, and its thickness increases over time. In Figure 8, magnetite powder is shown. There appears to be some cracking of the product shell, and an unreduced core is still present in the largest grains after 600 s of reduction.

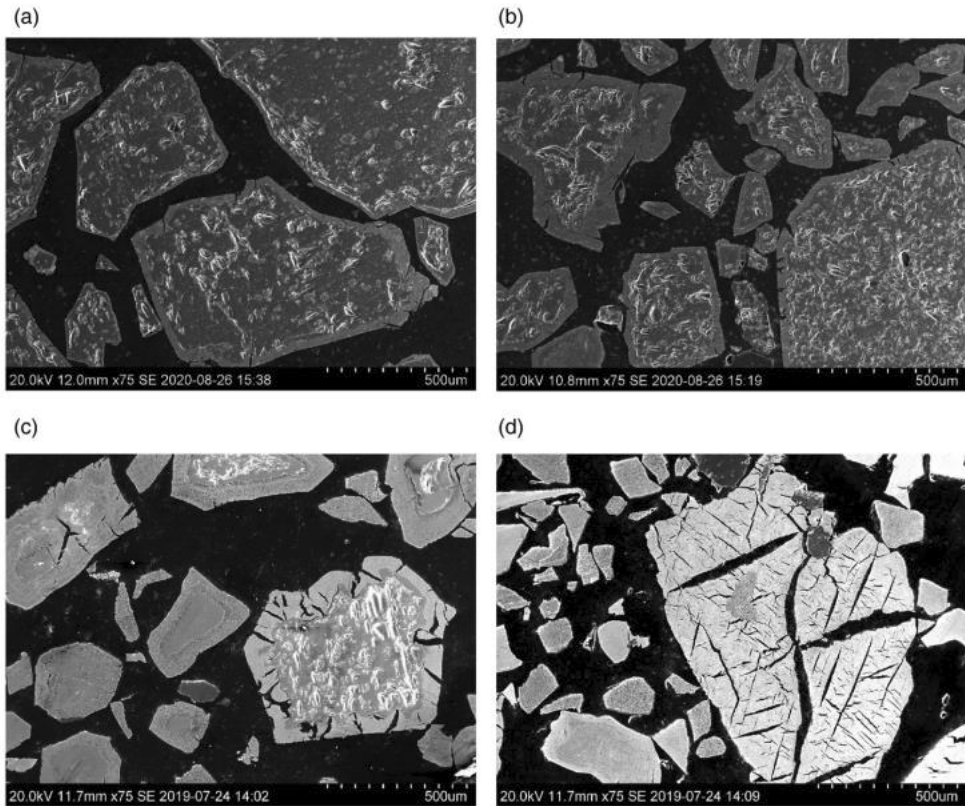


Figure 8 The progress of magnetite reduction at a temperature of 888 K after 30 s, (a); 60 s, (b); 120 s, (c); 600 s, (d).

In Figure 9, a partially reduced hematite powder is shown. The growth of the product shell over time is evident. After 600 s, an oxide core remains in the largest grain, much like the magnetite powder displayed. The similarities between the hematite and magnetite powders are evident. The main observable difference between the powders is the cracks in the product shell on the large magnetite grains. The product layer on the hematite grains does not appear to have the same crack propagation. However, for the smaller grains of magnetite, e.g., as seen in Figure 8 (c), the product shell characteristics are similar for both magnetite and hematite powders.

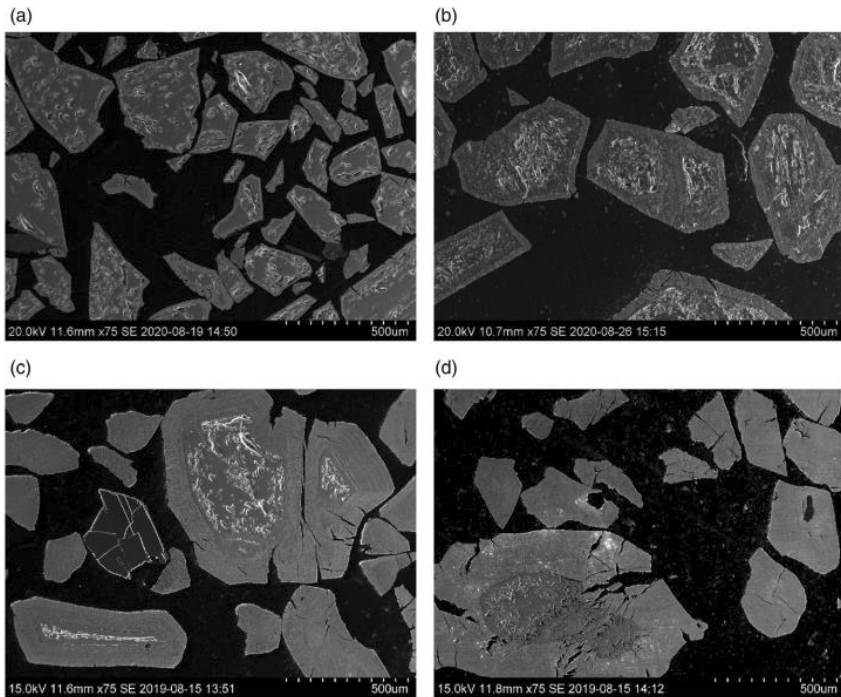


Figure 9 The progress of hematite reduction at a temperature of 888 K after 30 s, (a); 60 s, (b); 120 s, (c); 600 s, (d).

Looking closer at the early stage of reduction, Figure 10 shows both the hematite and magnetite powders at a larger magnification after 30 and 60 s reductions at 888 K. Clear layers of different products can be observed. After 30 s, iron can be seen on the surface of both powders. Furthermore, even a magnetite layer can be seen in the hematite powder. After 60 s, iron, wüstite, and magnetite layers can be observed in the magnetite powder; iron, wüstite, magnetite, and hematite can be observed in the hematite powder.

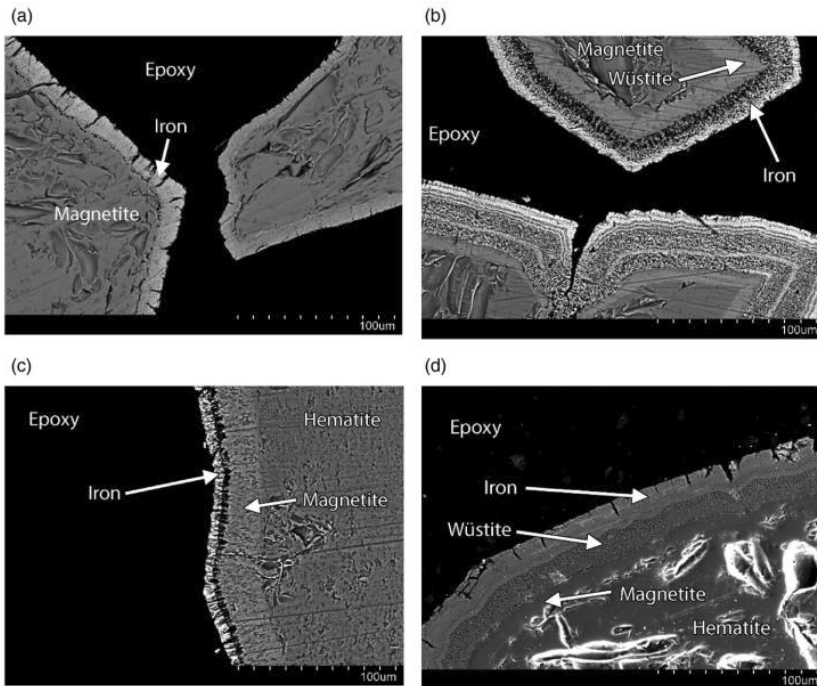


Figure 10 Micrographs of powders reduced at a temperature of 888 K. Magnetite powder is shown after 30 s in (a); and 60 s in (b). Hematite powder is shown after 30 s in (c); and 60 s in (d).

The temperature recorded in the bed is presented in Figure 11. The initial empty chamber temperature is visible in the first seconds of the temperature recording, and the rapid temperature drop marks when the cold powder is introduced to the chamber. The initial temperature increase is rapid, roughly 600 K in 30 s and the temperature continuously increases during the following 300 s, whereafter it stabilizes. These initial 300 s account for the majority of the reduction (>70% reduction degree at 888 K). The average temperature in this time interval is used as the experimental temperature.

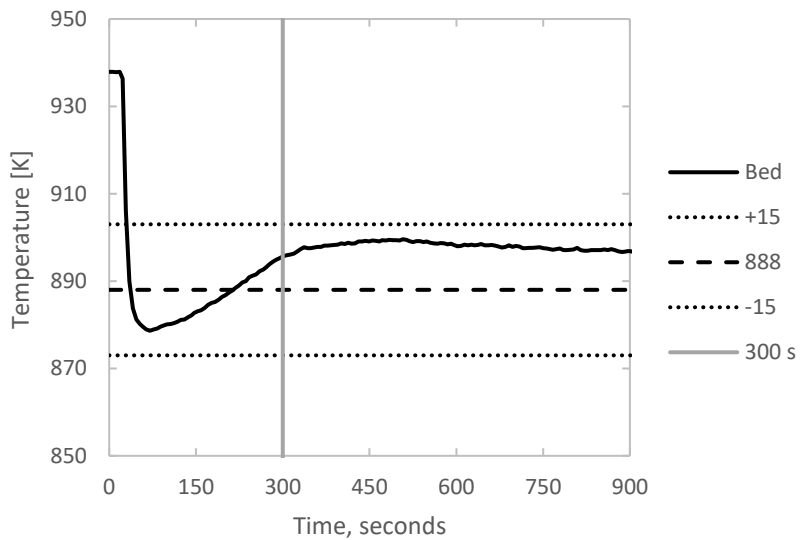


Figure 11 Temperature recorded in the bed during an experiment run at 888 K on magnetite fines.

4.2. Pellet microstructure

To investigate the reduction progression of pellets, experiments under different conditions were terminated at various reduction degrees. In Figure 12, the cross section of a pellet reduced to a 25 % reduction degree in a hydrogen atmosphere at 973 K is shown. SEM investigations were conducted to obtain micrographs along the pellet radius. At the pellet surface, Point A, grains appear to be porous throughout, and fully reduced iron could be observed: The reduction is ongoing throughout the grains, and it is even finished locally where iron is found. Further inside the pellet, Point B, the grain surfaces appear to be porous. However, no fully reduced iron was observed. The reduction is ongoing where the grains appear to be porous, but has not finished locally since no iron is found. The micrograph at the pellet center, Point C, clearly shows no trace of a porous structure. Therefore, two zones could be identified: Zone 1, where the reduction was ongoing, and Zone 2, where no reduction was observed. A dotted line was added to the figure to distinguish the zones; however, the position of the line is somewhat arbitrary since the transition between the zones was diffuse.

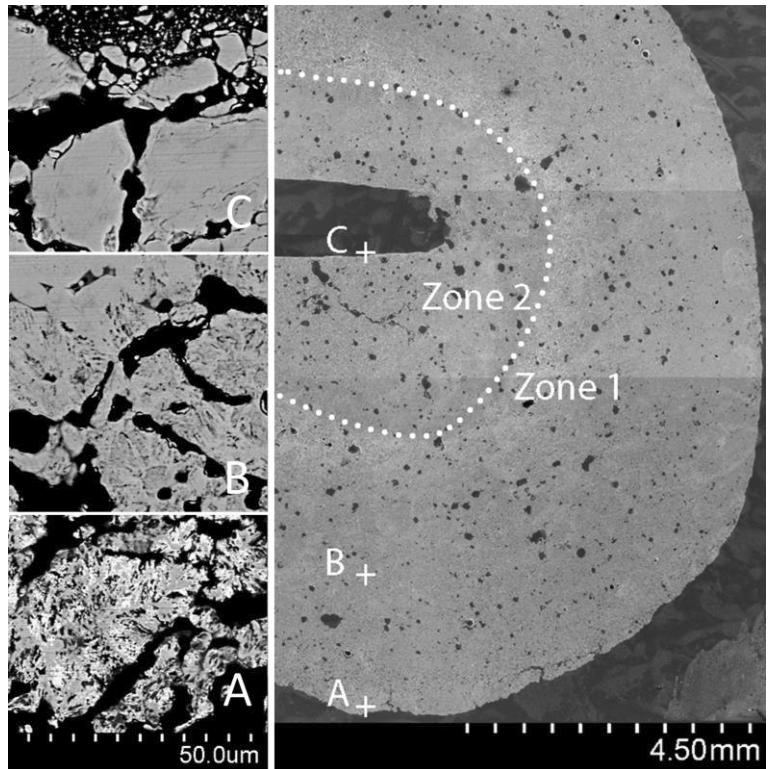


Figure 12 Cross-section of a hematite pellet reduced to 25 % at 973 K. A dotted line is added to distinguish between Zone 1, where reduction is occurring; and Zone 2, where no reduction could be observed. Three points along the pellet radius are also added, A, B, and C. Higher magnification micrographs taken at each point, are shown on the figure's left side.

To investigate the effect of temperature and water vapor on the grain microstructure, micrographs taken on cross sections of pellets reduced to 50 % reduction degree under various conditions are shown in Figures 13 to 16. Figure 13 show grains in the cross-section of a pellet at a 50 % reduction degree, at 873 K in pure hydrogen. In Figure 13 a), grains at a pellet's surface are shown. The structure appears to be porous, and no iron oxide is seen. The grains are fully reduced to iron. A micrograph from the center is shown in Figure 13 b). In the center part, a porous structure is seen on the grain surface, and pores can be observed throughout the grain. Pores indicate an ongoing reduction reaction, but no fully reduced iron is found.

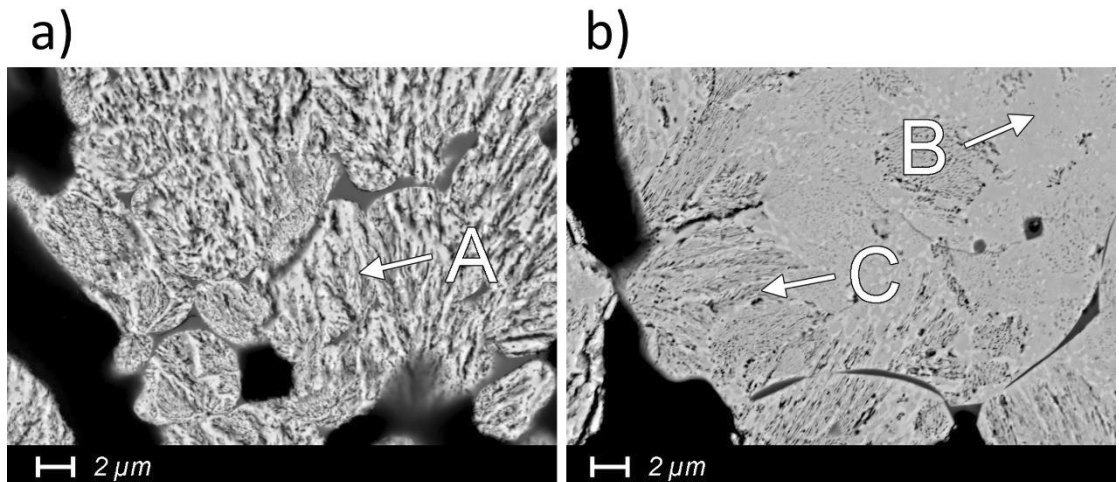


Figure 12 SEM micrograph taken on the cross-section of a pellet reduced to 50 % at 873 K in pure hydrogen. a) from close to the pellet surface, b) from the pellet center. A marks iron, and B and C marks iron oxides. The fine pore structure can be seen at position C.

When water is present during reduction at this temperature, the microstructure is changed. Figure 14 show grains in the cross-section of a pellet at a 50 % reduction degree, at 873 K in an atmosphere consisting of 85 % p_{H_2} and 15 % p_{H_2O} . Figure 14 a) is taken close to the pellet surface and shows that the structure is coarser as compared to the results in Figure 13 a). Furthermore, both iron and iron oxide can be seen. In Figure 14 b), the center is shown. Iron oxides are visible, marked B and C, and micro-pores perforate the grain. With 15 % p_{H_2O} , the micro-pore diameter is increased, and the number of pores is decreased compared to the case without water (as seen in Figure 13 b)).

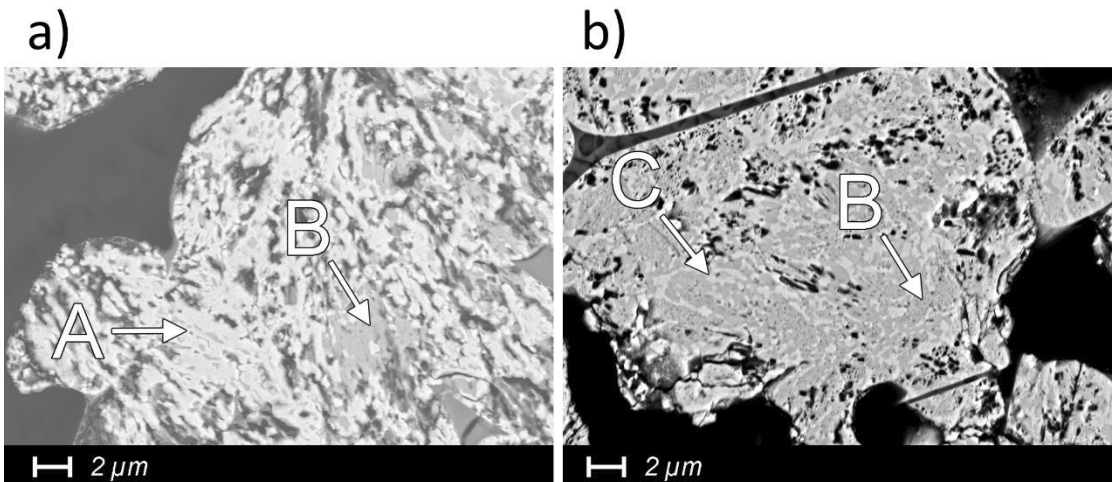


Figure 13 SEM micrograph taken on the cross-section of a pellet reduced to a 50 % degree at 873 K in 15 % p_{H_2O} , a) at the pellet surface, and b) at the pellet center. A marks iron, and B and C marks iron oxides.

Figure 15 show grains on the cross-section of a pellet reduced to 50 % reduction degree at 1173 K in a pure hydrogen atmosphere. Figure 15 a) show grains close to the surface, where fully reduced iron and iron oxide can be observed. The structure appears to be even more coarse, as compared to the results in both Figure 13 a) (873 K, 100 % p_{H_2}) and Figure 14 a) (873 K, 15 % p_{H_2O}), and the iron appears to form solid layers surrounding the oxides. In Figure 15 b), grains in the pellet center are shown. Pores and a mix of iron oxides are visible, but no solid iron layer is seen. The number of pores has decreased, and their diameter has increased compared to the pore structure seen in Figure 13 b) (center, 873 K, 100 % H_2).

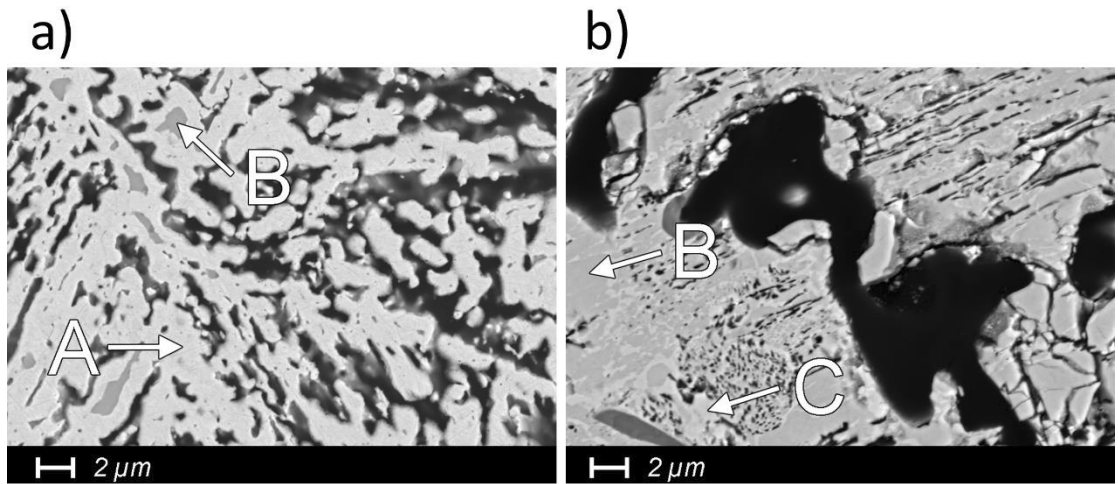


Figure 14 SEM micrograph taken on the cross-section of a pellet reduced to 50 % at 1173 K in pure hydrogen, a) at the pellet surface and b) at the pellet center. A marks iron, and B and C marks iron oxides.

Figure 16 shows micrographs from the cross-section of a pellet reduced to 50 % reduction degree at 1173 K in a hydrogen gas atmosphere with 15 % $p_{\text{H}_2\text{O}}$. Figure 16 a) shows grains close to the surface, the structure appears much the same as without water at the temperature, as observed in Figure 15 a). Iron is seen to form solid shells around the unreduced iron oxide. The iron oxide does not appear to be porous in this position at this temperature. In Figure 16 b), iron oxide grains are porous throughout, and no solid layers are observed. The number of pores appears to have decreased, and their diameters have increased compared to the pore structure seen without water in the atmosphere (as seen in Figure 15 b)).

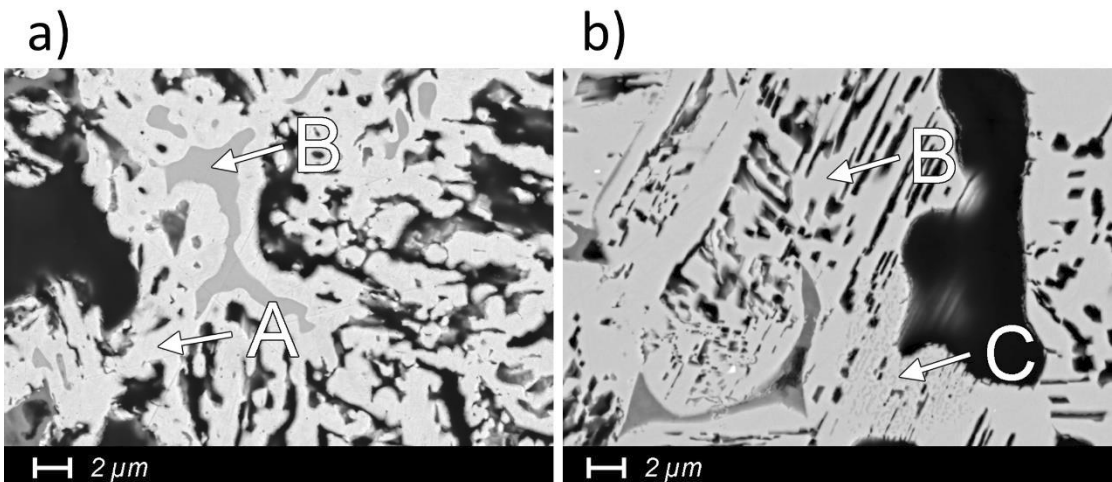


Figure 15 SEM micrograph from the cross-section of a pellet reduced to 50 % at 1173 K in 15 % $p_{\text{H}_2\text{O}}$, a) at the pellet surface and b) at the pellet center. A marks iron, and B and C marks iron oxides.

4.3. The effect of the endothermic reaction

In order to understand the impact of the endothermic reaction on the reduction, the pellet temperature was recorded during the reduction. The experiments were conducted with a thermocouple positioned in contact with the pellet surface and an additional thermocouple embedded in the pellet center. The temperatures recorded are reported in Figures 17 to 19. Figure 17 presents the first 450 s of temperature recordings from the experiments. The time for the surface to reach the experimental temperature can be noted; with an increasing temperature, the time to reach the target temperature is decreased. Also, the surface temperature rises more rapidly than the center temperature for all samples. Noting the temperature curve for 1173 K: The surface temperature of

the pellet reaches 1150 K in 100 s, and the center temperature reaches 1150 K in 250 s. After 300 s, the surface has reached 1173 K, and the center temperature is 1166 K. The center temperature reaches 1173 K after >800 s. Hence, it takes a significant amount of time for the center temperature to reach the surface and experimental temperature. This delay is most likely caused by the endothermic reaction, as will be discussed later in the thesis.

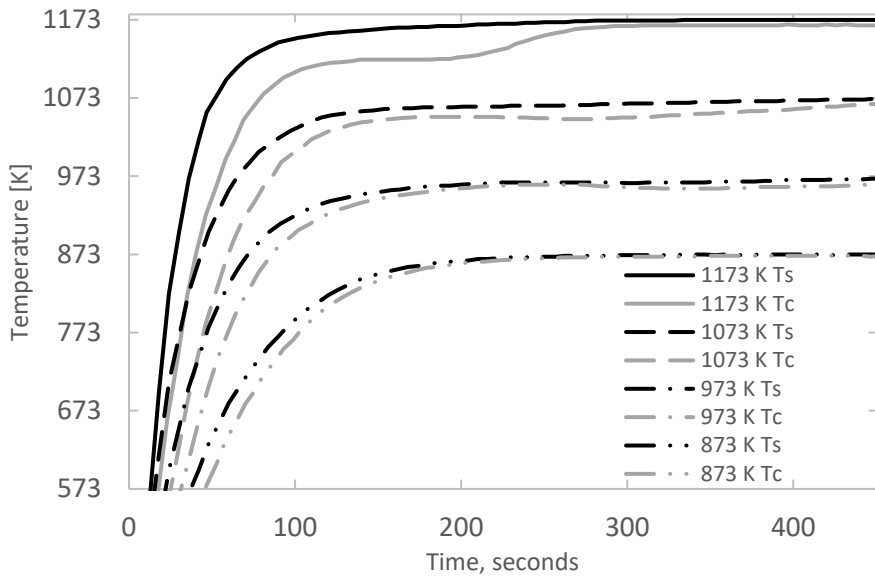
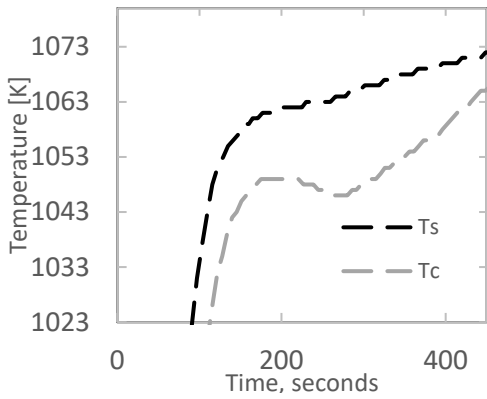
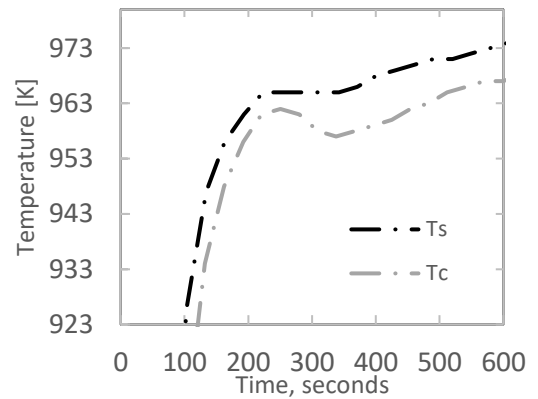


Figure 16 shows the temperature recorded at the pellet surface, T_s , and center, T_c , for reduction experiments in the 873–1173 K temperature interval.

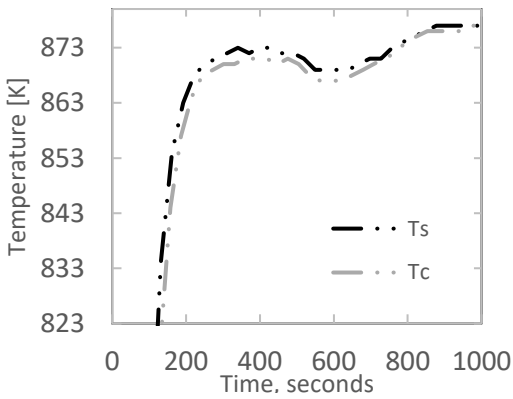
Figure 18 presents temperature recordings of the 1073 K, (a); 973 K, (b); and 873 K, (c) experiments, respectively, at a scale that enables a sufficient resolution in the relevant temperature interval. In the 973 K experiment, the surface temperatures show a plateau after roughly 250 s. In the 873 K experiment, the surface temperature shows a local maximum after 400 s, and a local minimum after 600 s. Also, the center temperatures recorded for all samples show a local maximum and minimum or a plateau at some point.



a) 1073 K experimental temperature. Ts, surface temperature, Tc center temperature



b) 973 K experimental temperature. Ts, surface temperature, Tc center temperature



c) 873 K experimental temperature. Ts, surface temperature, Tc center temperature

Figure 17 Temperature as measured by the thermocouple at the pellet surface, Ts; and center, Tc; for reduction at 873, 973, and 1073 K.

To be able to compare the temperature recordings obtained with this modified TGA method with previously published results, a conventional experiment was run in the setup. The temperatures recorded for both the conventional and alternative methods are presented in Figure 19. During the conventional experiment, the center and surface temperatures are 1173 K when the reactive gas is introduced at $t=0$. Roughly 100 s after the reactive gas is introduced, the center temperature begins to decrease. It reaches a minimum of 1135 K after

250 s, after which it begins to increase again. A stable temperature (<1 K/10 s) is reached after 400 s, at 1166 K (thereafter, the temperature increase is roughly 1 K/100 s). The center temperature reaches 1173 K after approximately 900 s.

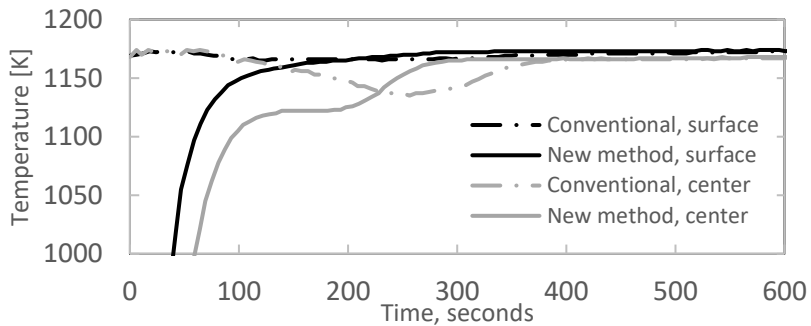


Figure 18 Temperature measured at pellet center and surface, for the conventional and the alternative method, respectively.

To understand when this temperature phenomenon impacts the reduction, the weight change of the pellet over time is simultaneously recorded. The reduction curves are presented in Figure 20. As the reduction progresses, a trend of a gradually declining reduction rate over time can be observed in the figure. The trend of an initially increasing reaction rate with an increasing temperature can also be observed.

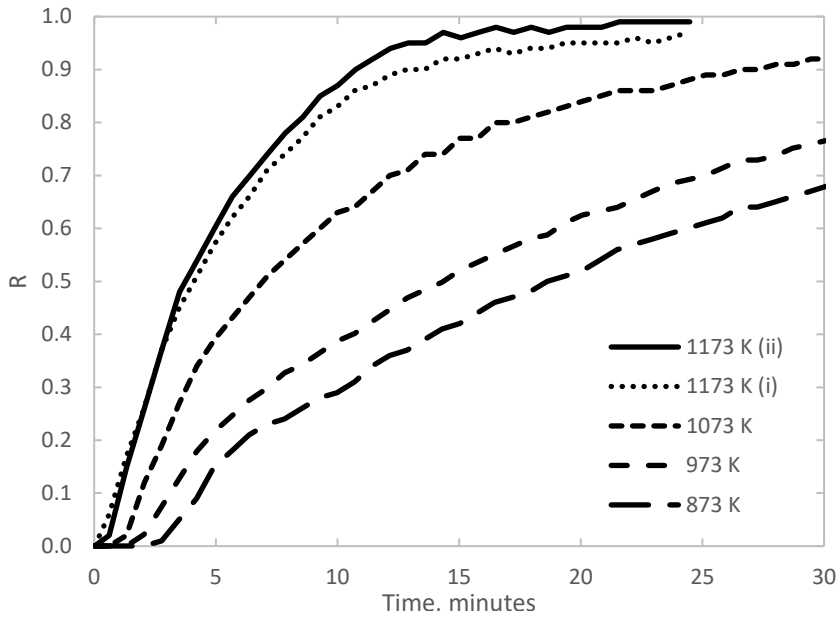


Figure 19 Reduction curves obtained from the experiments where the temperature was measured at the pellet surface and center.

Temperature data from Figures 17 to 19 are compared to the reduction curves in Figure 20 and summarized in Table 3. The period from which the center temperature stops to increase until it increases again will be referred to as the plateau region. The onset of the plateau, relative to the reduction degree, occurs later as the temperature increases. The time to reach the plateau end and time to achieve a 90 % reduction degree decreases with an increasing temperature. In addition, the temperature difference at the plateau increases with increasing temperatures. However, a correlation between the plateau end and the reduction degree is not clear.

Table 3 Values obtained from the temperature and reduction degree curves from the experiments run at the respective temperatures. Reduction degrees at onset (R_{onset}) and end (R_{end}) of the plateau region, the maximum temperature difference between surface and center temperature measured during the plateau (T_s-T_c), time of plateau end (t_{end}), and time to reach a 90 % reduction degree (t_{90}). The conventional method did not show a plateau; therefore, its values are reported for the temperature curve's inflection point, as measured by the inner thermocouple.

Temperature [K]	R_{onset}	R_{end}	T_s-T_c [K]	t_{end} [s]	t_{90} [s]
873	0.10	0.35	3	720	4200
973	0.15	0.33	9	470	3000
1073	0.22	0.41	18	310	1650
1173 a	0.26	0.39	38	170	750
1173 b	0.30	0.42	39	190	650
1173 conventional	0.34	0.34	35	260	870

4.4. TGA pellet reduction results

Together with microstructural and temperature analysis, TGA investigations were conducted to understand how the reduction proceeds. Generally, the reduction rate is initially fast and decreases over time, whereas the last portion of the reduction process is significantly slow.

4.4.1. The effect of water vapor

To study the influence of water vapor, experiments were conducted in a hydrogen atmosphere containing 0–15 % p_{H_2O} over the 873–1173 K temperature interval, the results are presented in Figures 21–24. The spread of curves indicates the significance of water in the atmosphere on the reaction rate at the specific temperature. The impact of water is pronounced at 873 K, Figure 21; there is a clear trend of a decreasing reaction rate with an increasing water content. In the temperature interval 973–1173 K, Figures 22–24, water is seen to lower the reaction rate, but the effect is less pronounced. Hence, the impact of water is lessened with an increased temperature. Comparing the time axes in Figures 21–24, the impact of temperature is seen; an increasing temperature decreases the reduction time.

In Figure 21, reduction curves obtained from experiments at 873 K are shown. The water contents tested were 0, 5, 10, and 15 % p_{H_2O} . As the water content increases, the reduction rate is significantly decreased.

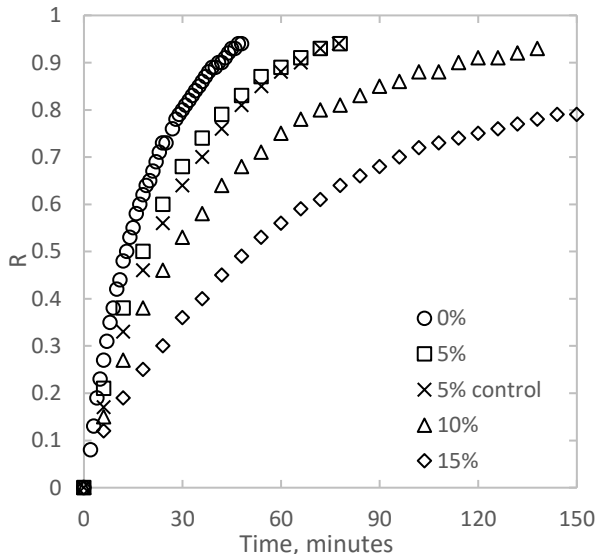


Figure 20 Reduction curves obtained from reduction experiments at an experimental temperature of 873 K with 0–15 % p_{H_2O} in the atmosphere.

Results from experiments run at 973 K are shown in Figure 21. A decrease in reaction rate is observed for all water vapor pressures. However, the gradually increasing water content does not clearly show a gradually increasing effect. All atmospheric compositions show a decreasing trend for the reduction rate as the reduction degree increases.

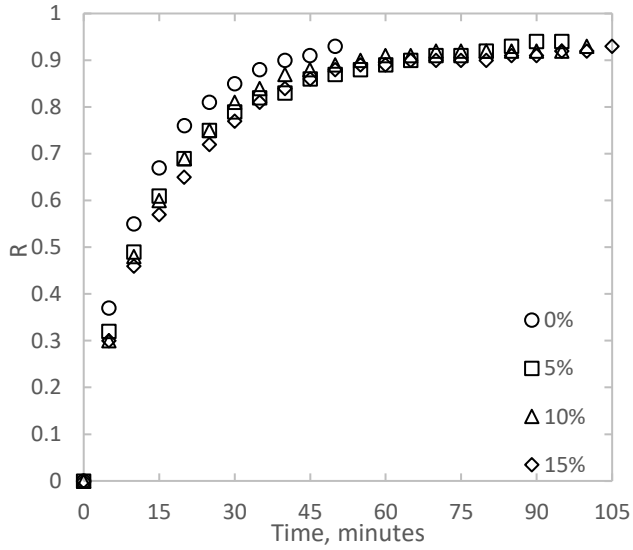


Figure 21 Reduction curves obtained from reduction experiments at an experimental temperature of 973 K with 0–15 % p_{H_2O} in the atmosphere.

Figure 23 show results from experiments run at an experimental temperature of 1073 K. The experiment run using an atmosphere containing 15 % p_{H_2O} is the most affected by water.

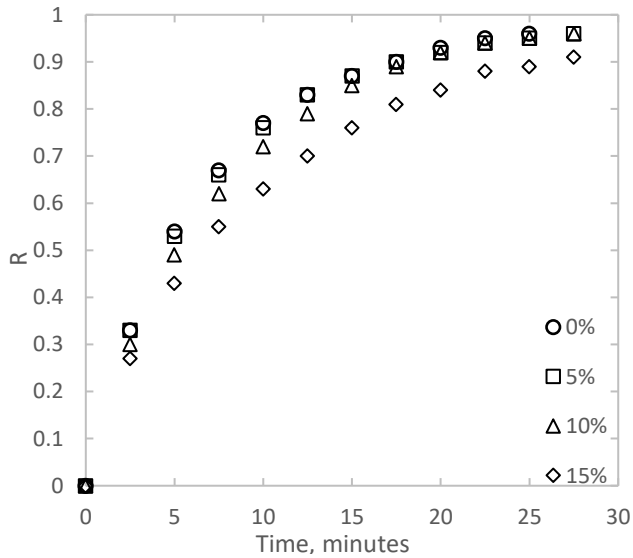


Figure 22 Reduction curves obtained from reduction experiments at an experimental temperature of 1073 K with 0–15 % p_{H_2O} in the atmosphere.

When the temperature is increased to 1173 K, a gradual effect of water is discernable again. All curves show the trend of a significantly lowered reduction rate as the reduction degree reaches levels above 90 %.

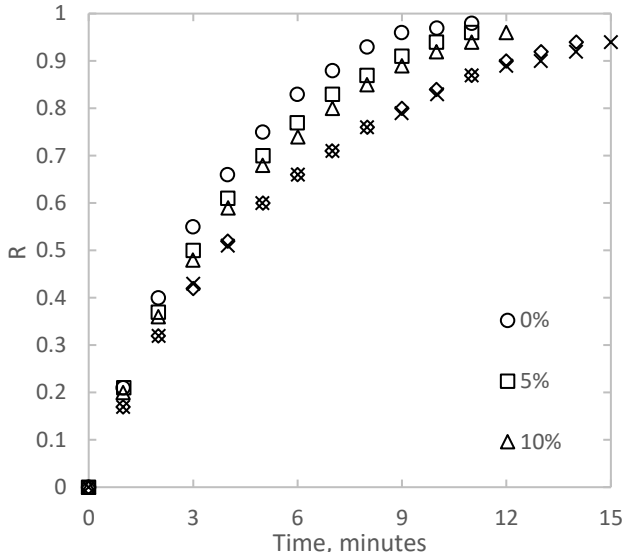


Figure 23 Reduction curves obtained from reduction experiments at an experimental temperature of 1173 K with 0–15 % p_{H₂O} in the atmosphere.

To investigate the influence of dilution, an experiment was run at 873 K using a 90 % p_{H₂} and 10 % p_{N₂} gas mix. In Figure 25, the result is compared to two previous reduction experiments conducted at the same temperature, one with a 90 % p_{H₂} and 10 % p_{H₂O} gas mix and one with pure hydrogen gas. The temperature was chosen because it was observed to be the most affected by the water content. When nitrogen is introduced, the reaction degree of the pellet at any given timestep is approximately 20 % lower compared to the reduction in pure hydrogen gas. When water is introduced, the reduction degree at the same timestep is roughly 40 % lower than that of pure hydrogen.

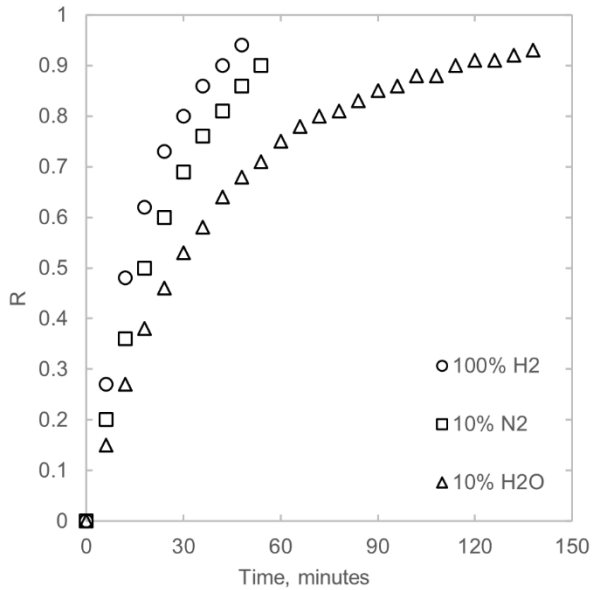


Figure 24 Reduction curves obtained from reduction at 873 K, with pure hydrogen atmosphere, or hydrogen mixed with 10 % p_{N_2} or 10 % p_{H_2O} .

4.4.2. Late stage reduction

The late stage is significantly slow compared to the rest of the reduction, as seen in previous figures (Figures 21 to 25). To gain insight into what happens during the late stage, experiments were conducted where the reduction was initiated at 1123 K and lowered to temperatures of 878, 923, or 973 K as the sample reached 80, 85, or 90 % reduction degrees. One reference experiment was run where the temperature was kept constant at 1123 K.

In Figure 26, the results from lowering the temperature at the 80 % reduction degree are presented. All samples are slower than the reference, and show a similar lowered reaction rate.

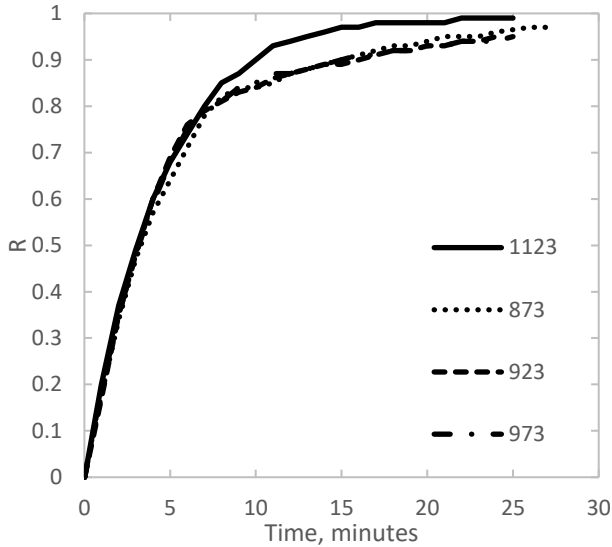


Figure 25 Reduction curves obtained from experiments conducted at 1123 K, where the temperature was reduced to 878, 923, and 973 K when the pellet reached an 80 % reduction degree. One reference sample is shown, reduced at 1123 K throughout.

Figure 27 shows the results of lowering the temperature of the samples at the 85 % reduction degree. Similarly to a lowering at an 80 % reduction degree (Figure 26), no clear difference can be seen between the samples when comparing the reaction rates after the lowering of temperature; all reaction rates are reduced by the same magnitude. In addition, all samples are seen to be slower when compared to the reference sample.

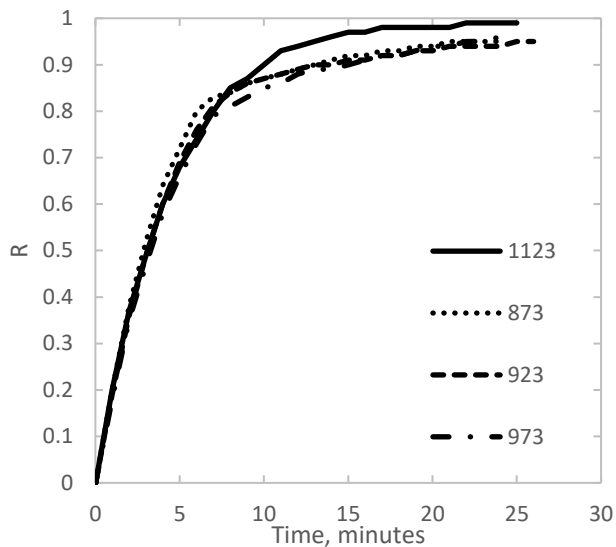


Figure 26 Reduction curves obtained from experiments conducted at 1123 K, where the temperature was reduced to 878, 923, and 973 K when the pellet reached an 85 % reduction degree. One reference sample is shown, reduced at 1123 K throughout.

The temperature was lowered as the sample reached a 90 % reduction degree in Figure 28. As seen in the figure, this does not seem to influence the reaction rate significantly compared to each other or the reference sample.

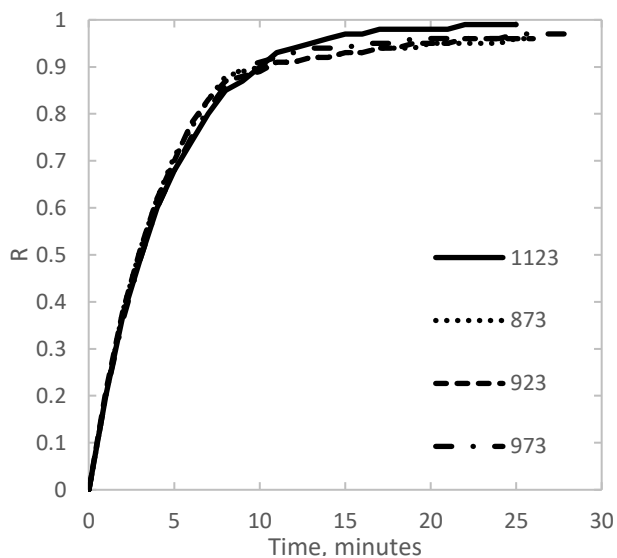


Figure 28 Reduction curves obtained from experiments conducted at 1123 K, where the temperature was reduced to 878, 923, and 973 K when the pellet reached a 90 % reduction degree. One reference sample is shown, reduced at 1123 K throughout.

4.5. Ore pellet properties

To investigate the effect of the ore pellet composition on its mechanical properties, the Cold Crushing Strength (CCS) was determined on 60 pellets of each composition, and the results are reported in Table 4. No clear trend could be observed.

Table 4 Pellet cold compressive strength.

[kg]	Pellet 1	Pellet 2	Pellet 3
CCS	314	320	308
Standard deviation	88	82	87

Pellets 1 and 3 were tested using the TGA setup under a pure hydrogen atmosphere. Reduction curves from the TGA experiments are reported in Figure 29. No significant difference could be discerned during reduction; the pellets show no significant difference with respect to the reducibility.

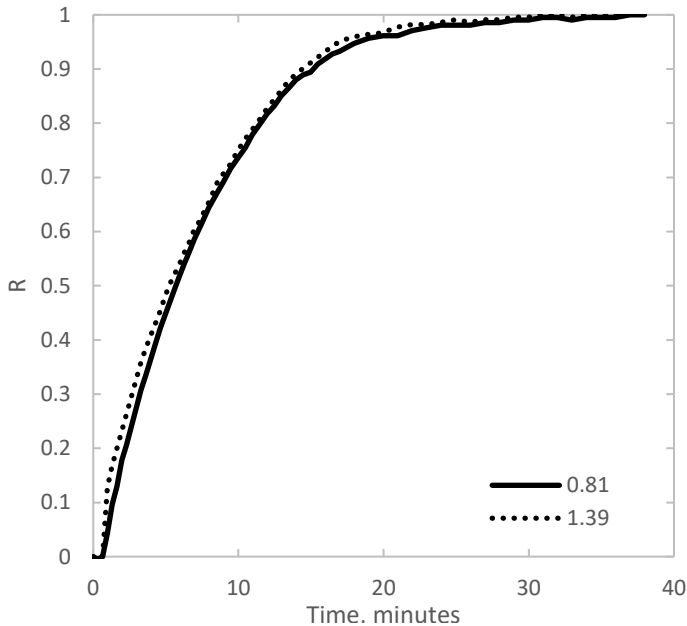


Figure 27 Reduction curves obtained from the TGA experiments on the pellets with 0.81 and 1.39 CaO/SiO₂ ratios.

Reduced pellets and discs were melted and cooled to investigate how the composition affects the slag's phosphorus refining capability. The samples were sent for OES and XRF determinations, and the results are presented in Table 4.

Table 4 Analysis results of the slag and metal phases of the systems after melting.

	Disc 1	Pellet 1	Pellet 2	Pellet 3	Disc 2
CaO/SiO ₂	0.24	0.62	0.97	1.16	2.32
P ₂ O ₅ slag [wt. %]	0.29	0.68	0.91	0.98	0.87
P iron [ppm]	360	180	120	90	15

The phosphorus partition between slag and metal, L_P , was calculated according to eq. (2),

$$L_P = \frac{2M_P \times (\text{wt}\% P_2O_5)}{M_{P_2O_5} \times [\text{wt}\% P]_{Fe}} \quad (2)$$

where M_P and $M_{P_2O_5}$ are the molar masses of phosphorus and phosphorus oxide, respectively. The variables $\text{wt.}\% P$ and $\text{wt.}\% P_2O_5$ are the phosphorus and phosphorus oxide concentrations in the metal and slag, respectively. The calculated L_P values are reported in Figure 30. Increased CaO/SiO₂ ratios increase the L_P values, as seen in the figure, which is in line with previous research results. [46–48]

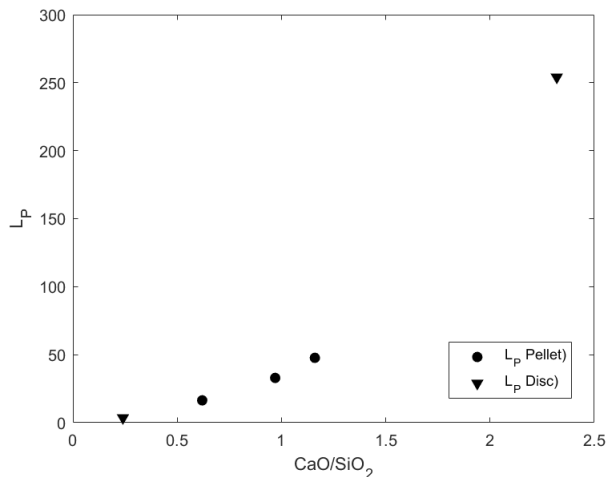


Figure 30 Phosphorus partition between slag and metal phase, L_P , obtained from the melting experiments. Data are given for both the pellet and disc systems.

5. Discussion

5.1. Repeatability and comparison to conventional methods

For the fluidized bed, each measuring point in Figure 6 and Figure 7 represents individual experiments. A good repeatability is shown at 300 s and 600 s, at 768 K and 888 K, respectively.

A pure hydrogen atmosphere without the gas switching step was desired. Considering the large contact area of the powders and rapid reaction, initial dilution effects in the commonly used fluidized bed experimental equipment might introduce considerable uncertainties. The present setup was designed to allow powders to be dropped directly into the reactor when the atmosphere and temperature had stabilized. Note, that the current setup could also be used to run experiments using the conventional method, viz. switching the inert gas to a reactant gas at a specific temperature. Additional experiments using the conventional method were also carried out in the setup to compare the two methods. In these runs, the powders were fluidized in inert gas and heated to the experimental temperature. Thereafter, a switch to a reactive gas was used to start the reaction. Finally, the reactive gas was switched back to an inert gas to stop the reaction before the furnace was ramped down.

The method of inserting the powders into a hot reactive furnace resulted in faster apparent reaction rates than the conventional method, as shown in Table 5.

Table 5 Reduction degrees obtained for the hematite powders reductions after 120 s at 768–933 K for the presently used experimental and conventional methods.

	768 K	838 K	848 K	888 K	933 K
New method	19 %	51 %		82 %	
Old method			43 %		59 %

The lower apparent reaction rates associated with the conventional method can have two causes: firstly, the lower partial pressure of hydrogen during the gas switching step, which would reduce the driving force for reduction. The exact gas composition during this period is unknown; it will go from 0–100 % reaction gas over a time scale relative to the experimental setup. Considering the timescale for the reduction, the period of gas switching can extend over a substantial amount of time. Secondly, the fluidization of particles in the hot inert gas could affect the powder's surface properties. While the first cause is

relatively straightforward, the second cause needs further study. It was investigated by Fruehan et al., where annealing was shown to provide lower apparent reaction rates for some ores but not for others. [35] Why certain ores are more affected by annealing is not elucidated. Hence, the possible effect on the surface properties before reduction would require serious consideration when the conventional fluidized bed is employed. A temperature drop in the furnace's hot zone is also associated with the reaction's onset in both methods. The temperature in the hot zone, as measured by the thermocouple, will go down when the cold powder is introduced. When the powder was hot, and the reactive gas was introduced instead, less or no temperature drop in the bed was expected. However, the temperature decreased by roughly 0.5 K/s during the initial 90 s. To the authors' knowledge, the observation of this drop has not been reported in the literature. More specifically, most authors have assumed the bed temperature to be constant and have not measured the temperature directly. Two common practices might mitigate this temperature drop. A low hydrogen concentration would lower the reaction rate and consume less heat momentarily. Also, inert powder added to the bed would store additional heat for the reaction. These practices are commonly found in the literature. [39, 60–63] Although these practices might minimize the temperature drop, they may introduce other uncertainties. Liu used a method like the one presently used, although with a mixture of iron oxide and alumina powder at a lower hydrogen partial pressure. [63] This makes a comparison of the results difficult.

In the TGA study, the use of industrial pellets would introduce some slight variations in composition, porosity, and geometry caused by the pelletization process. However, Figure 20, Figure 21, and Figure 24 show a reasonable repeatability.

Comparing the results from Figures 21–24 to Figure 20, the reaction rate is lower in Figure 20. This is caused by the lower gas flow in the furnace, 0.8 nl/min as opposed to 4 nl/min. The experiment did not allow for higher flows without disturbing the balance, because of the thermocouple wires inserted in the sample. Nonetheless, even at the lower flow, the reaction consumed enough energy to impact the reduction considerably. Note, the flow was extensively investigated for the other TGA studies to not limit the reduction by mass transfer in the gas phase.

The TGA experimental method employed in Supplements 2–5 differs from the conventional method in how the reaction is started. The conventional method starts the reaction on a pre-heated sample using an inert atmosphere by introducing a reactive gas. The method presently used starts the reaction by

introducing the sample to a pre-heated and reactive atmosphere of a fixed composition. The heating removes uncertainties introduced by the gas switch during the initial stage of the reaction. In such a manner, the sample is reduced during the whole period with a well-defined gas composition. It should be mentioned that the present setup also facilitates experiments using the conventional method. Therefore, additional experiments conducted with the conventional method were run in the setup for comparison. In these experiments, the samples were pre-heated in an argon gas atmosphere, and a switch to reactive gas started the reaction. Reactive gas was switched back to inert gas to stop the reaction, and the furnace was ramped down. As can be seen in Figure 31, the presently used method results in higher and more consistent reaction rates.

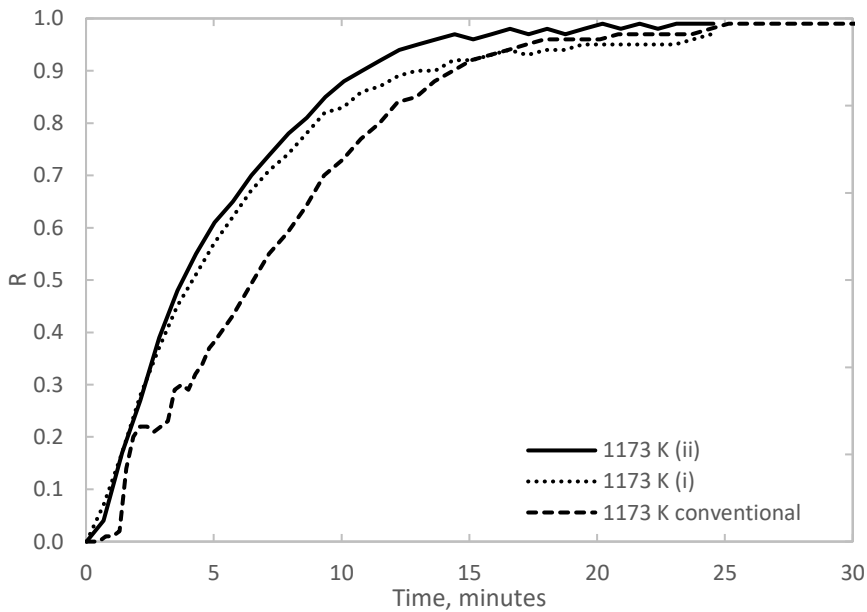


Figure 28 TGA curves obtained using the conventional method and the presently used method.

The results presented by Kazemi et al., when using the same method as employed in this work, also clearly show a higher initial reduction rate compared to the initial reaction rate obtained when using the conventional method. [12] This indicates that the gas switch would affect the reaction more

than the temperature increase. More specifically, the gas switch has a more profound effect on the reduction rate.

When using H_2 - H_2O gas mixtures, the gas composition was found to require a substantial amount of time to stabilize, measured by the vapor monitor at the furnace inlet. The presently used method was therefore essential to obtain an H_2 - H_2O gas mixture with a reliable H_2O content.

5.2. Fluidized bed

A fluidized bed setup was used to study the possibility of using fluidization in iron reduction. The results would also allow for the study of iron ore reduction at a grain level and compare hematite and magnetite fines. Figures 6 and 7 show the reduction curves obtained from the reduction experiments: At 300 s, the hematite powder has reached higher reduction degrees (72–85 %) than magnetite (58–71 %). At 600 s and 768 K, the hematite has reached a reduction degree of 78 %, while the magnetite has reached 63 %. After 600 s at 838 and 888 K; the hematite powder has reached 90 and 94 % reduction degrees, respectively; the magnetite powder has reached 87 and 91 % reduction degrees, respectively. After 900 s, the hematite powder has reached 86–95 % reduction degree, and the magnetite powder has reached values of 88–96 % for all temperatures. The hematite powder reduces slightly faster than hematite initially; this is especially true for reduction at 768 K. However, at 900 s, both powders have reached similar reduction degrees for all temperatures. The reduction trend is the same for both powders; the initial reduction is rapid (first 120 s at 888 K or 300 s at 768 K), and as the reduction degree approaches or exceeds values of 90 %, further reduction is slow. Mass transfer to the grain surface is not considered limiting since the flow is high, 0.75 m/s through the filter, and the bed is fully fluidized. Initially, mass transfer inside the grain is also considered to be fast and non-limiting because of the very short diffusion distance, e.g., the first couple of seconds of reduction. Figures 8 and 9 show the microstructure of fines at four different times during reduction. A product layer formed on the grain surface can be seen to move into the grain over time. When there is a lack of cracks or pores, as is usual for natural ores, the reduction starts at the surface and takes place layer-by-layer, as seen in Figure 10. Some cracking of the product shell was observed, which enabled diffusion through the openings. However, the amount of cracking was small, and the total effect was considered to be negligible. As the reduction proceeds, the reduction rate is seen to decrease gradually. With an increasing degree of reduction, the transport distances in the grains will increase, and the lowering

reaction rate is attributed to the increasing resistance to mass transfer through the growing product layer.

The heat transfer to the surfaces of the grains from the system is considered high, but it might still be influencing due to the endothermic nature of the reaction. The gas is pre-heated before it comes into contact with the bed, so the gas temperature entering the bed can be considered to be constant. However, the total heat supplied to the system is reactor dependent. Therefore, the temperature in the bed is monitored by a thermocouple. A characteristic temperature curve, recorded during an experiment, is shown in Figure 11. The chemical reaction consumes heat supplied by the furnace and the gas stream. As the temperature increases, the reaction rate increases in turn. As seen in Figure 11, the bed reaches a temperature of roughly 20–30 K below the gas temperature 10 s after the powder drop. After that, the temperature increase is slow, reaching the gas temperature 350 s later. If the heat supply to the system was non-limiting or there was no reaction occurring, the bed should not require 350 s to reach the gas temperature. The amount of heat supplied to the bed is always more than the heat consumed by the reaction. Therefore, the bed temperature continues to increase. However, the temperature increase is slowed in the 10–350 s interval because the endothermic reaction consumes the heat supplied. The 350 s needed to reach the gas temperature corresponds well to the reduction curves, where after 350 s, there is a significant slowing of the reduction rate. This reduction slowing is attributed to the increasing thickness of the product layers on the grains, slowing mass transfer and limiting the reaction. In the conventional method, where the powder was heated to the reaction temperature in an inert atmosphere, showed a temperature decrease when the reaction started. The decrease in bed temperature indicates that the reaction consumes more heat than what is supplied to the bed. This is due to the heat transferred into the grain being consumed at the reaction interface inside the grain.

In this setup, hematite and magnetite fines were found to reach a $\approx 90\%$ reduction degree in similar times. The results suggest that using magnetite powder in a fluidized bed reactor could be considered. However, much more systematic studies must be carried out to further investigate this aspect in detail.

5.3. Pellet reduction

To increase the knowledge of the reduction of iron pellets, a TGA setup was used to follow the reduction. Furthermore, SEM investigations of pellets at different reduction degrees were done to investigate the microstructure and understand the reaction mechanisms.

5.3.1. Mechanism

Micrographs of a pellet at a 25 % reduction degree from Supplement 2 are presented in Figure 12. The figure shows the reaction front before it has reached the pellet center. At point A, fully reduced iron and porous iron oxide grains are seen; at point B, no fully reduced iron is seen, but a porous zone extends from the grain surfaces towards the unreduced grain centers; at Point C, neither iron nor a porous structure is observed, no reduction is ongoing. Therefore, two general zones were identified in the pellet: Zone 1, where the reduction was ongoing, and Zone 2, where no reduction was observed. A dotted line was added in Figure 12 to show the zones. Since it is impossible to precisely determine the depth where no reduction has occurred in the pellet, the position of the line is somewhat arbitrary. Since fully reduced iron is seen at Point A but not at Point B, the grains are considered to be more reduced at Point A compared to Point B. The grains are more reduced further from the pellet's center, indicating that mass transfer along the pellet's radius is one of the rate-controlling mechanisms for reduction. The same behavior is seen for all reduction degrees, temperatures, and gas compositions being investigated.

In Zone 1, a mix of reduction reactions occurs at any given time. SEM investigations with EDS are not accurate enough to determine individual oxides. Therefore, the mixed structures found in Figure 12 (A) are assumed to contain iron during all reduction stages. Kim et al. show a pellet reduced at 973 K for two hours in hydrogen, investigated by EBSD, where hematite is still present in the pellet after the completed experiment. The structures found in their experiments correspond well with those found in pellets reduced in the current work. Their experimental results attest that a layer-by-layer reduction mechanism does not occur when reducing porous pellets. [64] This result contradicts some earlier works on pellet reduction, where clear layers are shown. [12,22,33] However, the results can be explained by the pellet pore structure, as also discussed by Turkdogan et al. [18] During the pelletization of industrial pellets, a significant amount of macro-pores are formed. These pores facilitate a radial gas diffusion and lower the diffusion resistance significantly, preventing the formation of layers. Many previous works have been conducted on denser pellets produced in a laboratory [16, 18, 19] or natural ores [18], in

which a lack of macro-pores causes a higher gas diffusion resistance, which results in the formation of layers.

SEM images of pellets reduced to 50 % from Supplement 3 are shown in Figures 13 to 16. Fully reduced iron grains can be observed at the pellet surface in Figure 13 a). Furthermore, the grains appear to be porous to their center. No fully reduced iron is found in the center of the same pellet, as shown in Figure 13 b). However, a porous zone extends from the grains' surfaces towards the grains' centers. Furthermore, the cores of some grains lack pores and appear to be unreduced. This indicates that grains are reduced from the surface inwards; indicating that mass transfer along the grain radius is another rate-controlling mechanism. The pellet and the oxide grains inside the pellet are reduced from the surface inwards, similar to grains in the fluidized bed.

In the study of the effect of the endothermic reduction reaction, Supplement 2, the reduction curves obtained from the TGA experiments show that the initial reduction is fast, e.g. Figures 21 and 26. The heating of the pellet surface is also fast, as recorded by the thermocouple in contact with the pellet surface in Figure 17. Note that in these experiments, the gas flow rate is low (0.8 nl/min); therefore, the mass transfer in the gas phase is still one of the rate-controlling steps. During this initial period, the reaction is mainly governed by the chemical reaction and mass transfer to the pellet's surface because of the short transport distances. Mass transfer to the pellet's surface is controlled by the flux of reaction gas in the chamber when the surface is unreduced. After some initial seconds in this regime, products have started to form on the oxide grains, and diffusion through them begins to influence the mass transport. As the reaction moves deeper into the pellet, the reactive volume increases, consuming more reactants and heat. The heat and mass transfer along the pellet's radius and grain diffusion begin to influence the reaction. The pellet center temperature mirrors the surface temperature initially. However, as the reduction progresses, it lags behind and stabilizes below the surface temperature. For a time, the center temperature ceases to increase entirely, or even decrease. The effect is most clearly visible in the 1173 K experiment in Figure 17 where a plateau of the center temperature is seen. The center temperature in this period (130–190 s of the experimental time) is roughly 40 K below the surface temperature, and the plateau prevails for roughly 60 s before the temperature begins to increase again. The surface temperature slowly increases during this time, and the surface temperature reaches the experimental temperature approximately 100 s after the center temperatures plateau ends. The temperature recorded for the 873–1073 K experiments are

shown in Figure 17 and Figure 18. The center temperature curves do not show a proper plateau. Instead, they describe a local maximum 200–400 s after the experiment was initiated, 3–18 K below the surface temperature at the time. 100–200 s later the center temperature displays a local minimum, approximately 3 K below the local maximum. After this, it slowly increases to the surface temperature. In the 973 K experiment, even the pellet's surface temperature is seen to plateau (at 965 K) for roughly 100 s. In the 873 K experiment, the surface temperature describes a local maximum (at 873 K) 400 s after the experiment was initiated. 200 s after this local maximum, a local minimum is seen (at 869 K), whereafter the surface temperature increases to 877 K over 400 s. The center temperature recorded for the 873 K experiment is consistently 4 K below the surface temperature until the local minimum is passed. The center temperature meets the surface temperature 700 s after the experiment was initiated. For all temperatures investigated, there appears to be a time during reduction where the pellet's local temperature either plateaus or decreases. For further discussion, the plateau region will refer to the time during reduction when the pellet's center temperature plateaus, or the time between its local maximum and minimum. Values for the plateau is shown in Table 3.

During this plateau, it is reasonable to assume that all heat transferred into the pellet was consumed by the reaction, hindering a further local temperature increase. A balance between the reaction rate and heat transfer occurred. An increased reaction rate would lower the center temperature, which in turn would decrease the reaction rate. Hence, the heat transfer was, at least in part, controlling the reaction rate. This period of heat transfer influence prevailed for a substantial reduction time, roughly from a 20 % to a 40 % reduction degree as seen in Table 3. One experiment was conducted at 1173 K using the conventional method, where the sample was hot, and the atmosphere changed from inert to reacting. During the same reduction degree interval, 20 % to 40 %, the effect is similarly recorded for the traditional method (described in detail in section 5.1 Repeatability and comparison to conventional methods). The pellet's center temperature goes down until a minimum is reached 35 K below the experimental temperature. After this, the temperature increases again as seen in Figure 19. During this reduced core temperature period, the reaction rates for both methods are similar as seen in Figure 31. Furthermore, the duration of the period (reduction degree of 26–42 % in the presently used method, 34 % for the conventional method) and the magnitude of the temperature drops (35–39 K) are also similar. It is, therefore, reasonable to

assume that the reduction is affected similarly by heat transfer in both methods. This aspect will be further discussed in the heat transfer part of the thesis.

At a certain point, the temperature in the pellet starts to increase again, indicating a decreasing heat transfer control and the pellet enters another mixed control regime. The reacting volume will begin to decrease as the surface finishes reducing, and the reaction moves even deeper into the pellet. The heat consumption will decrease as the reactive volume decreases, and the heat transfer will play a less important role. Heat transfer will still influence the reduction, but the increased distances for mass transport will increasingly influence it.

During the late reduction stage, the main barrier for reduction is expected to be diffusion. The reaction zone will be small in the pellet and grain centers. When the transport distance in the pellet is considerably long, the radial mass transport resistance will be high. Also, as seen from the fluidized bed experiments, grain diffusion will severely limit the reduction rate when the transport distance has increased beyond some point.

5.3.2. Temperature effect

Increasing temperatures increase reduction rates and decrease reduction times, as shown in Supplements 1–3 and shown in Figures 21 to 24. This is expected since the chemical reaction is sensitive to heat, as it is endothermic. The reaction requires heat, and an increased temperature increases the heat flux from the system to the sample. The backward reaction rate is also highly affected by heat, as discussed further in section 5.3.4 Effect of water content in the reaction gas.

There are observable changes in microstructure that occur with increasing temperatures. Comparing the cross-section at the surface of two pellets reduced to a 50 % reduction degree in a pure hydrogen atmosphere, at 873 K and 1173 K shown in Figure 13 a) and Figure 15 a), respectively: No iron oxide is found at the surface at 873 K, while there is iron oxide present at 1173 K. It is clear that the reduction is more extensive at the surface at 873 K compared to at 1173 K. Since the pellets are of the same reduction degree, this indicates that the reaction zone in the pellet is less expansive radially at the 873 K temperature than at 1173 K.

Porous iron is seen at 873 K, while solid iron is observed at 1173 K. St. John et al. have previously reported that the porous structure facilitates a direct contact of the reducing gas to the wüstite phase, while the solid layers impede

it. The reduction was observed to finish more rapidly when the porous iron was present compared to the solid iron. [45] In the case of pellets, solid layers slow down the mass transfer between the macro-pores and the reaction interface.

In addition, comparing the micro-pore structure in the pellet center without water at 873 K (Figure 13 b)) with 1173 K (Figure 15 b)), the increased temperature is seen to increase the pore diameter but decrease the number of pores. This is also true with water (Figure 14 b) and Figure 16 b)). This effect of temperature on the pore structure has also been reported by St. John et al. on wüstite fines and Matthew et al. on magnetite fines. [34, 45] A decreasing number of pores in the iron oxide will increase the distance for solid-state mass transfer.

No change was observed in the pellet macro-pore structure in Supplements 2 and 3. Since the macro-pores are formed during the pelletization, the pores are unaffected by the reduction. However, previous studies on compacts have shown that macro-pores decreased in diameter as the reduction temperature increased. [43,44] Those studies utilized lab-made compacts as opposed to industrial pellets. Therefore, the different effects could be due to the nature of the samples.

With increasing temperatures, the number of micro-pores in the oxide decreases, solid iron layers are formed, and the macro-pore structure remains unaltered. These effects combined allow the gas to penetrate deeper into the pellet with a retained reduction capacity, which causes a radially more expansive reduction zone with an increasing temperature.

This temperature effect is also interesting because diffusion is less sensitive to the temperature than the chemical reaction is. If the reaction rate is dominated by diffusion at the end of reduction, a temperature change should only have a minor effect on the reduction. As observed in the reduction curves in Figures 21 to 24, the reduction rate trend towards the end of reduction is significantly low. Therefore, experiments were run to study the effect of the temperature during the late stage of reduction. Samples were reduced at 1123 K and subsequently lowered in temperature to 873, 923, or 973 K at reduction degrees of 80, 85, or 90 %, as shown in Figures 26 to 28. An effect on the reduction rate is observable when the temperature is lowered at an 80 % reduction degree. The reduction rate is reduced when the temperature is lowered. On the other hand, lowering the temperature at the 90 % reduction degree has no significant impact on the reduction rate. The impact of lowering the sample temperature varies depending on the degree of reduction of the sample. This would indicate

that the reaction at the 80 % reduction degree is still jointly controlled by chemical reaction, diffusion, and even heat transfer. In comparison, above the 90 % reduction degree, the reduction is mainly controlled by diffusion.

5.3.3. Effect of the endothermic reaction

The temperature drop in the bed inspired the experiment where thermocouples were embedded in the pellet. Most authors assume that the heat transfer is fast enough to be negligible. However, as seen in the fluidized bed experiments, even heat transfer to the bed/grain could not be entirely neglected (Figure 11). The results of the experiments using the conventional method in the bed also revealed the same trend. The reaction consumes heat, leading to a lowered temperature if there is a lack of heat supplied. This, in turn, leads to a lowered reaction rate.

The impact of the plateaued core temperatures at 973 and 1173 K was estimated by calculating the chemical reaction rate quote between the pellet surface and center using the Arrhenius equation and the respective pellets' surface and center temperatures reported in Table 3. A wide range of activation energies for the reaction have been reported in the literature, 40–120 kJ, and the calculated results over the range are listed in Table 6. [40] As can be seen in the table, the ratio of reaction rate between center and surface can be in the range of 0.87–0.65 at 1173 K. At 973 K, the ratio is lowered to 0.95–0.86. There is a significant difference in the calculated reaction rate at the surface compared to deeper within the pellet, but the difference decreases with decreasing temperatures. One can, therefore, assume that there will be a difference in reaction rate at the surface compared to deeper within the pellet caused by the temperature difference alone. This is true for all reported activation energies.

Table 6 Calculated ratios of chemical reaction rate coefficients, K_r , for the temperatures recorded in the pellet center and the pellet surface during the plateau (values calculated with the listed activation energy).

Activation energy [kJ]	40	60	100	120
$K_{r_{1133\text{ K}}}/K_{r_{1173\text{ K}}}$	0.87	0.80	0.70	0.65
$K_{r_{963\text{ K}}}/K_{r_{973\text{ K}}}$	0.95	0.93	0.88	0.86

In addition, the apparent thermal conductivity of the pellet was calculated using the data from the plateau period. Since the temperature did not increase, all heat transferred into the pellet could be assumed to be consumed by the

reaction and directly related to the pellet's conductivity and the thermal gradient, eq (3),

$$\frac{dn}{dt} \Delta H = -4\pi r^2 k \frac{\partial T}{\partial r} \quad (3)$$

where dn/dt is the reaction rate in moles (moles/s), ΔH is the reaction enthalpy (J/mole), r is the radius of the spherical reaction interface (m), k is the thermal conductivity (W/mK), and dT/dr is the temperature gradient (K/m). Assumptions made to enable the calculations were the following: reaction at time t was localized to a spherical shell inside the pellet with the radius r , a full reduction had occurred between the pellet's surface and r , no reduction had occurred from r to the pellet's center, the temperature distribution was linear from the pellet's surface to r , and the temperature was constant from r to the pellet's center. Because of these assumptions, the thermal conductivity is called an apparent conductivity. Based on eq. (3), the assumptions mentioned above, and the experimental data provided in Table 3, linear regression was used to calculate the apparent thermal conductivity of the pellet. The results are presented in Table 7 for the respective temperatures.

Table 7 Calculated range of apparent thermal conductivities for 600–900 °C.

Isothermal temperature [K]	Range of apparent thermal conductivity [W/mK]
873	4.02 to 3.19
973	4.10 to 1.87
1073	2.73 to 3.76
1173	1.10 to 1.25

The resulting apparent heat conductivities of 1–4 W/mK are one order of magnitude lower than that of pure iron, which is reported to be approximately 40 W/mK. [68] This was expected because of the porous nature of the reduced zone.

A similar phenomenon was observed in the fluidized bed experiments. The reaction consumes enough heat to limit the temperature increase in the bed. Comparing the reduction curve of the fluidized bed to the temperature curve recorded in the bed, Figure 6 and Figure 7 to Figure 11: the temperature gradually increases during the first 300 s of reduction, and this time corresponds to approximately a 80 % reduction degree. During this time, the reduction is fast and can be assumed to be under a chemical or a mixed control.

The bed temperature stabilizes when the reactive volume in the particles has decreased enough for the system to become diffusion-controlled.

5.3.4. Effect of water content in the reaction gas

To investigate the effect of water during reduction, experiments were run in the TGA setup, in the 873–1173 K temperature interval, using a hydrogen gas atmosphere, and with a water vapor content of 0–15 %. Some samples were reduced to a reduction degree of 50 % and examined in the SEM to see if the microstructure was altered and how the reduction progressed. Starting with the microstructure at 873 K: When using a pure hydrogen atmosphere, the grains at the pellet surface appear to be porous throughout, and only iron is found, as seen in Figure 13 a). When 15 % water was added to the atmosphere, the grains were also porous, although the structure appear coarser than without water in the atmosphere, Figure 14 a). Some iron oxide was also seen in the center of larger grains, roughly 8–9 microns from the grain surface. Notably, the time to reach a 50 % reduction degree in a pure hydrogen atmosphere at the temperature required 12 min; whereas with 15 % water vapor in the atmosphere, the time to reach the same reduction degree was 48 min. However, SEM investigation of the grains at the surface of a pellet reduced to a 95 % reduction degree (60 min) in pure hydrogen atmosphere at the same temperature revealed no significant coarsening over time. Hence, the time spent at the temperature did not cause the coarser structure. Moving to the microstructure at 1173 K: With a pure hydrogen atmosphere, a solid shell can be seen to have formed on the grain surface, roughly 1–2 microns thick, surrounding an iron oxide center, Figure 15 a). With 15 % water vapor added to the atmosphere, Figure 16 a), the microstructure is similar to the structure seen without water, shown in Figure 15 a); no change in microstructure can be observed at the pellets surface. However, a coarsening of the micro-pore structure can be observed in the pellet center. Micro-pores have increased in diameter and decreased in number as the $p_{\text{H}_2\text{O}}$ value increases from 0 to 15 %, as seen when comparing the structures in Figure 15 b) with Figure 16 b). Microstructural changes occurring during the reduction of magnetite and wüstite fines with increasing $p_{\text{H}_2\text{O}}$ values have previously been investigated by St. John et al. and Matthew et al. An increase of the $p_{\text{H}_2\text{O}}$ value was found to coarsen the micro-pore structure formed in the iron oxide grains during reduction. In addition, porous iron product layers were reported to form in pure H_2 for all temperatures (723–1373 K), while solid iron layers were reported to occur at elevated $p_{\text{H}_2\text{O}}$ values. [34, 45] The solid layers presently observed when reducing in pure H_2 could result from locally elevated $p_{\text{H}_2\text{O}}$ values caused by the reduction reaction.

With added water at 873 K, the coarser structure formed could cause an increased diffusion resistance. It is reasonable to assume that this resistance would increase with an increased transport distance as the reduction progresses. However, the reduction is severely affected by water throughout, even initially when transport distances can be considered short, as seen in the reduction curves at the temperature (Figure 21). One could, therefore, argue that the microstructure is not solely responsible for the slowing effect of the water.

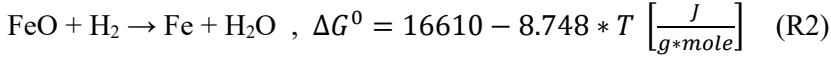
In addition to causing a coarsened microstructure, water will dilute the hydrogen gas. Consequently, this decreases the partial pressure of reactants and increases the partial pressure of products in the system. This should, in turn, affect the reaction rate. Altering the partial pressures of reactants and products in the system will influence both the driving force for diffusion and the chemical reaction rate. A TGA experiment was run on a pellet where the gas was diluted by adding 10 % nitrogen to investigate and separate the dilution effects. The nitrogen reduction curve is compared to an experiment with 10 % water vapor and a reference using pure hydrogen gas in Figure 25. It shows that, compared to the reference, the iron ore pellet was roughly 20 % less reduced at any given timestep with nitrogen in the atmosphere; while with water, the pellet was approximately 40 % less reduced at the corresponding time.

Diffusion is known to be a function of material properties, temperature, and the concentration gradient set by the local partial pressures of elements. Since the system has a fixed total pressure, diluting the reactive gas will affect the driving force for diffusion by altering the diffusional gradient between the pellet surface and the reaction interface. As hydrogen is consumed at the reaction interface, additional hydrogen must be transported to the reaction interface for the reduction to continue. If the partial pressure of hydrogen outside the pellet is lowered, the diffusional gradient to the reaction interface will be decreased, which will slow the mass transport. This is one part of the dilution effect on diffusion caused by both water and nitrogen. Since water will be produced at the reaction interface, water will have a concentration gradient from the reaction interface to the pellet surface. If the water content outside the pellet is increased, the concentration gradient of water towards the pellet surface will be decreased, which is an effect on mass transport that nitrogen does not have.

As mentioned earlier, water will also affect the chemical reaction rate in addition to the altered driving force for diffusion. To discuss water's influence

on the chemical reaction kinetics, the thermodynamics of the reaction needs to be addressed. Since the micrographs show a mixed reaction zone, all reduction steps can be assumed to occur simultaneously in the pellet. Therefore, the wüstite reduction is chosen as an example for further discussion.

The driving force for the chemical reaction (R2) can be found in the literature: [65]



It is known that the dG^0 value can be determined through eq. (4);

$$\Delta G^0 = -RT \ln(K) \quad (4)$$

where R is the gas constant, T is the temperature, and K is the equilibrium constant, satisfying the expression shown in eq. (5):

$$K = \frac{p_{\text{H}_2\text{O}}^e}{p_{\text{H}_2}^e} \quad (5)$$

$p_{\text{H}_2\text{O}}^e$ and $p_{\text{H}_2}^e$ are the equilibrium pressures of water and hydrogen, respectively. The reaction rate is commonly written as shown in eq. (6):

$$\frac{dx}{dt} = k_f * A_f * p_{\text{H}_2} - k_b * A_b * p_{\text{H}_2\text{O}} \quad (6)$$

where k_f and k_b are the forward and backward reaction rate constants, A_f and A_b are the areas available where the forward and backward reactions can take place, and p_{H_2} and $p_{\text{H}_2\text{O}}$ are the partial pressures of the reactants and products, respectively. From eq. (6) one can observe that the total reaction rate directly depends on the availability of reactants and products. A decreased partial pressure of hydrogen will decrease the size of the forward reaction rate portion, as caused by either water or nitrogen dilution. Dilution by water will also affect the backward reaction rate, while nitrogen dilution does not. If the areas in eq. (6) are considered equal and we write the equation at the equilibrium; the equation can be written as follows, eq. (7):

$$\frac{p_{\text{H}_2\text{O}}^e}{p_{\text{H}_2}^e} = \frac{k_f}{k_b} = K \quad (7)$$

Calculated values for k_b/k_f and K for the experimental temperature range (873–1173 K) are presented in Table 8.

Table 8 k_b/k_f and K calculated in the 873 to 1173 K temperature range.

	873 K	973 K	1073 K	1173 K
k_b/k_f	3.4	2.7	2.2	1.9
K	0.29	0.37	0.44	0.52

The substantial retardation of reaction at 873 K, as seen in the experiments, is seen in the calculated values as well. The backward reaction rate constant at 873 K is more than three times the size of the forward reaction rate constant. At 1173 K, the backward reaction rate constant is less than twice the size of the forward constant. The total reaction rate is much more affected by the $p_{\text{H}_2\text{O}}$ value at low temperatures than at high temperatures. Increasing the H_2O content will increase the backward reaction, decreasing the total reaction rate. The presence of H_2O in the reactor gas will also decrease in the p_{H_2} value, further decreasing the total reaction rate. The increase of the k_b/k_f ratio with decreasing temperatures results in more profound effects of water at lower reaction temperatures. The lowered chemical reaction rate at an increased water content, along with the increased resistance to grain diffusion due to the coarsened micro-pore structure, will push the reaction deeper into the pellet through the macro-pores. This will cause the more expansive reduction zone with high $p_{\text{H}_2\text{O}}$ compared to low $p_{\text{H}_2\text{O}}$ as observed at 873 K.

5.4. Pellet properties

The reducibility and mechanical properties of the three pellets were investigated (one was produced to represent the LKAB KPRS pellet as a reference). All pellets were manufactured using the same procedure because the pelletizing process and the composition influence the pellet properties.

No significant difference is observed in the pellet strength or reducibility when the composition is altered, as seen in Table 4 and Figure 29. However, the small changes in composition significantly affected the phosphorus distribution upon melting. It is, therefore, reasonable to expect that pellet modifications within the investigated CaO/SiO_2 ratio interval could greatly improve the dephosphorization power of the autogenous slag while retaining the pellet's properties.

Pellets were molten, and the metal and slag compositions were analyzed. As clearly seen in Figure 30, the phosphor content in the slag and the metal varied depending on the ingoing composition. With only bentonite additions, as tested with the Disc 1 system, the resulting slag had the lowest CaO/SiO_2 ratio of all

systems investigated. The phosphorus content in the metal phase was measured at 360 ppm. The slag formed upon melting of the Disc 2 system had the highest CaO/SiO₂ ratio, and the amount of phosphorus in the metal phase was below the detection limit of the OES analysis (< 20 ppm). For the pellets, the phosphorus content was lowered from 180 ppm to 90 ppm when the CaO/SiO₂ ratio increased from 0.81 to 1.39. Increasing the CaO/SiO₂ ratio increased phosphorus content in the slag, in line with previous research on the subject. [58,66,67] What is interesting to note in this study is the time frame. The reduced materials spend approximately 2 min in a fully molten state, which is too short a time for the assumption of thermodynamic equilibrium between top-slag and metal to be reached. The compositions represented here range from only a bentonite binder addition to a relatively large amount of calcium oxide addition. The finely dispersed non-ferrous oxides melt to form a slag phase with a large contact area to the metal phase. The short transport distance and large contact area enable a fast mass transfer between the phases. The phosphorus is located in an apatite phase in the ore gangue grains for these materials. As the gangue melts, the apatite dissolves, and the phosphorus is dispersed in the slag phase. [51] When molten slag and metal are in contact, phosphorus can transfer from the slag to the metal phase. The slag formed from a low CaO/SiO₂ ratio system (e.g., Disc 1, 0.31 CaO/SiO₂), the phosphorus readily migrates to the metal (resulting in 360 ppm of phosphorus in the metal phase). However, the slag can also hinder this transfer when the CaO/SiO₂ ratio is high (e.g., Disc 2, 2.4 CaO/SiO₂, resulting in <20 ppm in the metal phase). This mass transfer occurs in the short time frame under which the material melts. This implies the possibility of developing a pellet capable of achieving acceptable phosphorus levels upon melting in the EAF.

6. Concluding discussion

The thesis aimed to investigate some aspects of the direct reduction of iron ore in hydrogen. Today, direct reduction of iron ore is conducted via two major routes: the fluidized bed and the shaft process. Even though the majority of direct reduction industrially is conducted in the shaft using pellets, the fluidized bed, and fines were also investigated. Industrial pellets and fines were used to bring the research closer to industrial applications.

A laboratory fluidized bed system is utilized to investigate the difference between magnetite and hematite fines. Magnetite and hematite powder are reduced at three temperatures (Supplement 1). Figure 6 and Figure 7 show similar trends of reduction for both powders. The initial reduction is rapid, and the last reduction stage is slow. Both powders require similar and long times to

reach high reduction degrees (e.g., after 900 s at 768 K, they reach 86 and 89 % reduction degrees, respectively. After 900 s at 888 K, they reach 95 and 96 % reduction degrees, respectively). As seen in the SEM micrographs in Figure 8 and Figure 9, an increasingly thick product layer forms as the reduction progresses. The resistance to mass transfer through this layer will increase with its increasing thickness, and the slow reduction in the late stage was attributed to the layer formation. No whisker formation nor agglomeration was observed. The temperature in the bed was also affected during the reduction process, as seen in Figure 11. As the reaction is endothermic (R2), it will consume heat, and the temperature effect is attributed to the chemical reaction.

Since the majority of reduction today is conducted in the shaft furnace, more of the thesis focus is put there. Furthermore, since the endothermic reaction had a clear effect on the reduction in the fluidized bed, it could also affect the pellet reduction. Therefore, the chemical reaction was experimentally and theoretically studied in pellets in Supplement 2. A TGA setup was designed to simultaneously follow both the weight and the temperature of a pellet during reduction. The temperature is recorded at the surface and center simultaneously. The temperature in the center is seen to be lower than the surface temperature. The temperature difference varies with temperature. At 1173 K, the temperature difference is as high as 39 K; at 873 K, the difference is 3 K. The lower center temperature persists for a significant portion of reduction, e.g., during the reduction degree interval of 25–40 % at 1173 K or 10–35 % at 873 K, as seen in Figure 17, Figure 18, and Table 3. This is attributed to the chemical reaction together with the heat transfer in the pellet. The calculated apparent heat conductivity in the pellet is found to be significantly lower than that of pure iron, namely 1–4 W/mK compared to 40 W/mK. SEM investigations show a mixed reaction zone caused by the porous nature of the pellet, Figure 12. The combined effect of the porous pellet and the mixed reaction zone is considered to be the cause for the low calculated apparent thermal conductivity (1–4 W/mK). The effect of temperature on the apparent reaction rate is also calculated, and the results are presented in Table 6. It is clear that the temperature difference alone could cause the reaction rate to vary considerably over the pellet radius. At 1173 K, the ratio of center to surface reaction rate is 0.87–0.65, caused by the temperature difference alone, depending on which activation energy is chosen for the calculation.

During reduction in a shaft, not only the temperature but also the water content will vary over the height. Hot hydrogen gas is introduced in the bottom, and

cold iron ore is introduced in the top. The gas temperature will also decrease and the $p_{\text{H}_2\text{O}}$ value will increase towards the top of the shaft as a result of the ongoing reduction. Therefore, understanding both the influence of temperature and water content on the reduction is crucial. Thus, this is the focus of Supplement 3. Specifically, the effect of water is investigated by reducing pellets in the TGA setup in a hydrogen gas atmosphere containing 0–15 % $p_{\text{H}_2\text{O}}$ over the 873–1173 K temperature range. The reduction curves in Figures 21 to 24 show a retarding effect of water for all investigated temperatures, but the results are most pronounced at 873 K. SEM investigations also show a change in the microstructure when water was present, Figures 13 to 16. Such a change can influence the reduction process. However, the change in microstructure cannot fully account for the slowing effect seen throughout the reduction period, especially during the early stages when diffusion distances are assumed to be short. Since water is the gaseous product of the reduction reaction, the $\text{H}_2\text{O}/\text{H}_2$ ratio can impact the reaction. The calculated ratios for the kinetic reaction rate constants in Table 8 show a significant impact of water vapor on the backward reaction rate, which increases with decreasing temperatures. For the wüstite reaction, the ratio of the backward reaction rate constant to the forward reaction rate constant is calculated to be 3.4 at 873 K and 1.9 at 1173 K. These results reveal that the backward reaction rate is the major contributor to the slowed reaction rate at 873 K.

As seen in the reduction in the fluidized bed, Figure 6 and Figure 7, and during the TGA experiments on pellets, Figures 21 to 24, the reduction rate trend significantly decreases towards the last part of the reduction process. Since the goal of the industrial reduction process will be to achieve a high yield from the iron ore, reaching high reduction degrees is important. However, the extended time in the reactor at high temperatures with low gains in yield will not be optimal for maximized productivity. Therefore, optimizing the process during this last part is important, which led to the study reported in Supplement 4. Diffusion is considered very important in this period, but the impact of temperature on diffusion is low, while its effect on the chemical reaction is high. Figures 26 to 28 show the temperature's influence on reduction above a reduction degree of 80 %. When the temperature is lowered at the 80–85 % reduction degrees, the reduction trend is slowed compared to the reference (Figure 26 and Figure 27). Therefore, the pellets at the 80–85 % reduction degrees are still considered to be under a mixed control from the chemical reaction, diffusion, and even heat transfer. However, at a 90 % reduction degree, the lowered temperature has no significant effect on the trend (Figure 28). Thus, the reduction is considered to be dominated by diffusion. The results

show that the reduction does not significantly benefit from a high temperature when the reduction degree is above 90 %. Consequently, this part of the reduction can be conducted at lower temperatures. In addition, the 90–100 % reduction degree interval is considerably long in view of the total process time. Decreasing the temperature in this interval could significantly reduce the total energy required for the process, lowering the process cost.

The reduction degree is not only important to increase the yield of iron ore, but also for the process that follows where the DRI is to be molten, e.g., in the EAF. The primary goals for the EAF process, when using hydrogen-reduced DRI, are to melt the ingoing materials and to perform a phosphorus refining. Increasing the reduction degrees of the DRI decreases the total energy required for melting due to the decreasing iron oxide content. In addition, an increased iron oxide content in the slag increases the amount of slag modifiers needed to obtain the desired phosphorus refining. Interestingly, Vickerfält et al. and Huss et al. show that the kinetic conditions potentially occurring in a pellet during the melting stage could aid in reaching a low phosphorus content. [49–51] However, the research was conducted on reduced iron ore pellets of a single composition. Therefore, Supplement 5 was focused on investigating the possibility of increasing the usefulness of the iron ore pellet by investigating the effect of pellet composition on its properties—specifically, the impact of gangue, binder, and fluxing oxides which form the primary slag upon melting. CCS testing of the pellets with 0.8, 1.2, and 1.4 CaO/SiO₂ ratios showed the pellets' strengths to be 314±88, 320±82, and 308±87 kg, respectively. Thus, no significant difference in pellet strength was found considering the standard deviation. In addition, no significant difference was found with respect to reducibility, as seen in Figure 29. Lime and dolomite were added to the ore mix to produce the pellets. Both these additives decompose at elevated temperatures and were reported in the literature to have detrimental effects on the mechanical strength of the compacts. However, the substances are also reported to increase the reducibility of the pellet due to their decomposition. [52–59] An increase of the CaO content should, therefore, increase the reducibility but lower the mechanical strength. Neither of these effects were observed in the current pellets. However, the previous studies were conducted on compacts made in a laboratory, and the nature of the samples might be the cause of these conflicting observations. [52–59] Figure 30 shows the impact of the CaO/SiO₂ ratio on the phosphorus refining upon melting. Two additional compositions were tested in the form of discs to expand the ratio interval and their data are also included in the figure. An increase in the CaO/SiO₂ ratio increases the phosphorus partition, increasing the phosphorus in the slag. It is

known that the CaO/SiO₂ ratio impacts the phosphorus partition, but it is also known that it affects the physical properties. The results show the possibility of altering the pellet composition without causing detrimental effects on the mechanical properties or reducibility.

Overall, the results show that the following six rate-controlling mechanisms can influence the pellet's reduction: (1) Mass transfer to and from the pellet surface: A lower gas flow in the furnace (0.8 nl/min instead of 4 nl/min) or lowered hydrogen content (by diluting the hydrogen with 10 % N₂) lowered the reduction rate. (2) Heat transfer to the pellet's surface. (3) Radial mass transfer in the pellet. (4) Radial heat transfer: The pellet's surface temperature was measured to be higher than the center, and the center temperature plateaued when the reaction consumed all heat transferred into the pellet. (5) Grain mass transfer: Grains were seen to be more reduced on their surfaces than deeper within. (6) Chemical reaction: The reduction was highly affected by atmospheric water vapor. The rate-controlling mechanism varies with reduction degree, temperature, and gas composition due to their impact on diffusion, heat transfer, and chemical reaction. A single mechanism seldom controls the reduction of pellets during the reduction. Only for the last few percent of the reduction, the main controlling step is diffusion.

The present results are hoped to aid in developing and optimizing the fluidized bed and shaft furnace processes, and shed some additional light on the controlling mechanisms of iron ore reduction by hydrogen.

7. Conclusions

The main results of the this thesis may be summarized as follows:

- Hematite and magnetite powders were reduced in a fluidized bed.
 - Hematite and magnetite powders showed similar trends of initially fast reductions, and slow reductions when reduction degrees were high. They both reached high reduction degrees in similar times, e.g., after 900 s; reaching reduction degrees of 86–89 % at 768 K, or 95–96 % at 888 K.
 - The late reduction stage is controlled by diffusion through a growing product layer.
- Pellets were reduced in a TGA setup.
 - The endothermic reaction influences the reduction during a significant portion of the reduction process. The most significant

- effect is seen in the reduction degree span of 10–40 %, but it also depends on the temperature.
- Calculated apparent heat transfer coefficients for the pellet are significantly lower (>90 %) than that of dense iron.
 - Microstructure changes with temperature and $p_{\text{H}_2\text{O}}$ values, and the diffusion rate will be altered because of the altered microstructure.
 - Water affects the reduction at all temperatures, where the most significant slowing effect is seen at 873 K.
 - The backward reaction is responsible for the significant retardation at 873 K, and its influence decreases with increasing temperatures.
 - During the last 10 % of reduction, diffusion dominates the reduction process.
- Three pellets, with CaO/SiO₂ ratios of 0.8, 1.2, and 1.4, were investigated.
 - Cold crushing strengths were measured to 308 ± 88 , 320 ± 82 and 314 ± 87 kg, respectively. No significant change in cold crushing strength was found relative to the CaO/SiO₂ ratio.
 - The 0.8 and 1.4 CaO/SiO₂ ratio pellets did not show significant differences during isothermal TGA reduction experiments in hydrogen. No significant change in reduction behavior was found relative to the CaO/SiO₂ ratio.
 - As the pellets were molten, the phosphorus content in the metal phase decreased with increasing CaO/SiO₂ ratios, resulting in 180, 120, and 90 ppm, respectively. The systems investigated in the form of discs with CaO/SiO₂ ratios of 0.3 and 2.4 resulted in phosphorus contents in the metal phases of 360 and < 20 ppm, respectively. The CaO/SiO₂ ratio greatly affects the phosphorus refining capability of the slag upon melting.

8. Suggestions for future work

In the shaft furnace, hydrogen will be introduced in the lower part of the shaft, while iron ore is introduced at the top. The gas exits at the top and the reduced iron exits at the bottom. Heating of the burden is usually done by introducing a hot reaction gas. The reaction is endothermic, consuming the heat in the gas. Therefore, the bottom of the shaft will have a higher temperature than the top since the reaction will cool it. The reaction products will also travel upwards with the gas. Therefore, the bottom of the shaft will have a low water content, and the top will have a high water content. As the pellet travels down through the shaft, it will experience an increasing temperature and decreasing water

content. As has been presented, the reduction of the pellet is affected by both temperature and gas composition. The effect of the water content during a non-isothermal reduction should be theoretically studied.

Since the reaction consumes heat and produces water, it would be important for the shaft furnace process to study how the pellets influence each other through heat transfer and gas distribution.

The present work has used only the LKAB KPRS pellet; in the future, iron ore from additional producers should be studied.

More studies on the fluidized bed powder should be done; how does the powder morphology change over time if suspended in an inert gas? It would also be interesting to investigate the effect of temperature on the grain microstructure, comparing hematite to magnetite. The SEM work conducted was focused on the microstructure at 888 K. However, it would be interesting to investigate the 768 K structure, as at this temperature, there is a difference in reduction degree after 600 s between the two powders.

9. Sustainability

This work can contribute to the global body of work conducted for UN STG-9.4, retrofitting current industries to make them sustainable. The thesis focuses on using hydrogen as a replacement for fossil fuels. By aiding in implementing this technology, the industry can be retrofitted to a more sustainable practice. If this thesis can aid in optimizing the process and increase its resource-use efficiency, this would also correspond well with the goal. [69]

UN STG-9.4: "By 2030, upgrade infrastructure and retrofit industries to make them sustainable, with increased resource-use efficiency and greater adoption of clean and environmentally sound technologies and industrial processes" [69]

Suppose the thesis can aid in optimizing the reduction process, creating less waste by achieving higher reduction degrees and utilizing the intrinsic gangue material in the ore for phosphorus refining. In that case, the work also contributes to achieving more sustainable and efficient use of natural resources, UN STG 12.2. [70]

UN STG-12.2: "By 2030, achieve the sustainable management and efficient use of natural resources" [70]

10. References

- [1] IEA, Energy Technology Perspectives, 2020. Available from: https://iea.blob.core.windows.net/assets/7f8aed40-89af-4348-be19-c8a67df0b9ea/Energy_Technology_Perspectives_2020_PDF.pdf [accessed 2024-02-20].
- [2] IEA, Global Energy Review 2019, 2019. Available from: https://iea.blob.core.windows.net/assets/dc48c054-9c96-4783-9ef7-462368d24397/Global_Energy_Review_2019.pdf [accessed 2024-02-20].
- [3] M. Bailera, P. Lisbona, B. Peña, L. M. Romeo, J. CO2 Util., 2021, 46, pp. 101456.
- [4] H. Y. Sohn, Metals, 2020, 10(1), p. 54.
- [5] Worldsteel Association, 2023 World Steel in Figures, 2023. Available from: [unesid.org/descargas_files/World-Steel-in-Figures-2023.pdf](https://www.worldsteel.org/unesid.org/descargas_files/World-Steel-in-Figures-2023.pdf) [accessed 2024-02-20].
- [7] Metso:Outotec, Fine Ore Direct Reduction Circored. Available from: <https://www.metso.com/globalassets/pdfs-and-other-downloads/circored---fine-ore-direct-reduction.pdf> [accessed 2024-02-20].
- [8] M. Sun, K. Pang, Z. Jiang, X. Meng, Z. Gu, J. Sustain. Metall., 2023, 9(4), pp. 1399–1416.
- [9] J. F. Gransden, J. S. Sheasby, Can. Metall. Q., 1974, 13(4), pp. 649–657.
- [10] F. Lu, L. Wen, H. Zhong, J. Xu, S. Zhang, H. Duan, Z. Yang, J. Appl. Crystallogr., 2018, 51(6), pp. 1641–1651.
- [11] O. Edström, J. Iron Steel Inst., 1953, 175, pp. 289–304.
- [12] M. Kazemi, B. Glaser, D. Sichen, Steel Res. Int., 2014, 85(4), pp. 718–728.
- [13] M. Kazemi: KTH Royal Institute of Technology, Stockholm, 2016, PhD Thesis.
- [14] D. Wagner, O. Devisme, F. Patisson, D. Ablitzer, Adv. Process. Met. Mater. Sohn Int. Symp., 2006, 2, pp. 111–120.
- [15] F. Patisson, O. Mirgaux, Metals, 2020, 10(7), pp. 921–936.

- [16] E. Kawasaki, J. Sanscrainte, T. J. Walsh, *AIChE J.*, 1962, 8(1), pp. 48–52.
- [17] A. Pineau, N. Kanari, I. Gaballah, *Thermochim. Acta*, 2006, 447(1), pp. 89–100.
- [18] E. T. Turkdogan, J. V. Vinters, *Metall. Mater. Trans. B.*, 1971, 2, pp. 3175–3188.
- [19] R. Takahashi, J. Yagi, Y. Omori, *Sci. Rep. Res. Inst. Tohoku Univ. Ser. A*, 1971, 57(10), pp. 1597–1605.
- [20] Y. Man, J. Feng, *Powder Technol.*, 2016, 301, pp. 1213–1217.
- [21] D. Gao, M. Hu, C. Pu, B. Xiao, Z. Hu, S. Lui, W. Xun, X. Zhu, *Int. J. Hydrog. Energy*, 2015, 40(14), pp. 4733–4740.
- [22] M. Kazemi, M. Saffari Pour, D. Sichen, *Metall. Mater. Trans. B.*, 2017, 48, pp. 1114–1122.
- [23] A. Ranzani da Costa, D. Wagner, F. Patisson, *J. Cleaner Prod.*, 2013, 46, pp. 27–35.
- [24] Z. Chen, J. Dang, X. Hu, H. Yan, *Metals*, 2018, 8(10), p. 751.
- [25] B. Weiss, J. Sturn, S. Voglsam, *Ironmak. Steelmak.* 2011, 38(1), pp. 65–73.
- [26] X. Mao, X. Hu, X. Cao, Y. Fan, K. Chou, *JOM*, 2023, 75(7), pp. 2745–2752.
- [27] M. Wiberg, *Jernkontorets Annaler* 124, 1940, 5, pp. 179–212.
- [28] W. M. McKewan, *AIME*, 1961, 221, p. 140.
- [29] J. Pang, P. Guo, P. Zhao, *J. Iron Steel Res. Int.*, 2015, 22(5), pp. 391–395.
- [30] W. Pluschkell, H. Yoshikoshi, *Arch. Eisenh.*, 1970, 41(8), pp. 715–721.
- [31] P. Garg, X. Hu, Y. Li, K. Li, S. Nag, J. Zhang, *Metall. Mater. Trans. B*, 2022, 53(3), pp. 1759–1774.
- [32] W. H. Kim, S. Lee, S. M. Kim, D. J. Min, *Int. J. Hydrog. Energy*, 2013, 38(10), pp. 4194–4200.
- [33] K. Sato, Y. Nishikawa, I. Tamura, *Trans. Iron Steel Inst. Jpn.*, 1983, 69(10), pp. 1272–1279.

- [34] S. P. Matthew, P. C. Hayes, *Metall. Mater. Trans. B.*, 1990, 21, pp. 153–172.
- [35] R. J. Fruehan, Y. Li, L. Brabie, E. J. Kim, *Scand. J. Metall.*, 2005, 34(3), pp. 205–212.
- [36] K. Piotrowski, K. Mondal, H. Lorethova, L. Stonawski, T. Szymanski, T. Wiltowski, *Int. J. Hydrog. Energy*, 2005, 30(15), pp. 1543–1554.
- [37] D. H. St. John, P. C. Hayes, *Metall. Mater. Trans. B.*, 1982, 13, pp. 117–124.
- [38] D. H. St. John, S. P. Matthew, P. C. Hayes, *Metall. Mater. Trans. B.*, 1985, 16, p. 857.
- [39] B. Weiss, J. Sturn, S. Voglsam, S. Strobl, H. Mali, F. Winter, J. Schenk, *Steel Res. Int.*, 2010, 81(2), pp. 93–99.
- [40] D. Spreitzer, J. Shenk, *Steel Res. Int.*, 2019, 90(10): 1900108.
- [41] Y. Hara, M. Tsuchiya, S. I. Kondo, *Trans. Iron Steel Inst. Jpn.*, 1974, 60(1), pp. 1261–70.
- [42] P. K. Strangwa, S. Toppis, H. U. Ross, *Can. Metall. Q.*, 1966, 5(3), p. 211.
- [43] A. Hammam, Y. Li, H. Nie, L. Zan, W. Ding, Y. Ge, M. Li, M. Omran, Y. Yu, *Min., Metall., Explor.*, 2021, 38, pp. 81–93.
- [44] Z. Wang, M. Chu, Z. Liu, Z. Chen, X. Xue, *J. Iron Steel Res. Int.*, 2012, 19, pp. 7–10.
- [45] D. H. St John, P. C. Hayes, *Metall. Mater. Trans. B.*, 1982, 13, pp. 117–124.
- [46] K. Balajiva, A. G. Quarrell, P. Vajragupta, *J. Iron Steel Inst.*, 1946, 153, p. 115.
- [47] K. Balajiva, P. Vajragupta, *J. Iron Steel Inst.*, 1947, 155(4), pp. 563–567.
- [48] E. T. Turkdogan, *ISIJ Int*, 2000, 40(10), pp. 964–970.
- [49] J. Huss, M. Berg, N. Kojola, *Metall. Mater. Trans. B.*, 2020, 51(2), pp. 786–794.
- [50] J. Huss, A. Vickerfält, N. Kojola, *Steel Res. Int.*, 2023, 94: 2300064.

- [51] A. Vickerfält, J. Huss, J. Martinsson, D. Sichen, *Metall. Mater. Trans. B*, 2023, 54(4), pp. 2206–2215.
- [52] M. K. Mohanty, S. Mishra, B. Mishra, S. Sarkar, *Arab. J. Sci. Eng.*, 2018, 43(11), pp. 5989–5998.
- [53] R. K. Dishwar, O. P. Sinha, *Fuel*, 2021, 296.
- [54] S. Dwarapudi, C. Sekhar, I. Paul, Y. G. S. Prasad, K. Modi, U. Chakraborty, *Ironmak. Steelmak.*, 2016, 43(3), pp. 180–191.
- [55] T. Umadevi, P. Kumar, N. F. Lobo, M. Prabhu, P. C. Mahapatra, M. Ranjan, *ISIJ Int.*, 2011, 51(1), pp. 14–20.
- [56] M. Iljana, A. Kemppainen, T. Paananen, O. Mattila, E. Pisilä, M. Kondrakov, T. Fabritius, *Int. J. Miner. Process.*, 2015, 141, pp. 34–43.
- [57] Y. Shi, D. Zhu, J. Pan, Z. Guo, S. Lu, M. Xu, *Powder Technol.*, 2022, 408, p. 117782.
- [58] J. Li, H. An, W. Liu, A. Yang, M. Chu, *J. Iron Steel Res. Int.*, 2020, 27(3), pp. 239–247.
- [59] E. T. Turkdogan, J. V. Vinters, *Can. Metall. Q.*, 1973, 12(1), pp. 9–21.
- [60] J. Yu, Y. Han, Y. Li, *Minerals*, 2017, 7(11) p. 209.
- [61] I. René, B. Olivares, University of New South Wales, 1989, PhD Thesis.
- [62] H. Baolin, H. Zhang, L. I. Hongzhong, *Chin. J. Chem. Eng.*, 2012, 20(1) pp. 10–17.
- [63] W. Liu, J. Y. Lim, M. A. Saucedo, *Chem. Eng. Sci.*, 2014, 120, pp. 149–166.
- [64] S. H. Kim, X. Zhang, Y. Ma, I. R. Souza Filho, K. Schweinar, K. Angenendt, D. Raabe, *Acta Materialia*, 2021, 212: 116933.
- [65] P. C. Hayes, *Process Principles in Minerals & Materials Production*, Hayes Publishing, Brisbane, Australia, 1993, 638. ISBN978-0958919722.
- [66] S. Basu, A. K. Lahiri, S. Seetharaman, *Metall. Mater. Trans. B*, 2007, 38(3), pp. 357–366.
- [67] A. Vickerfält, J. Martinsson, D. Sichen, *Steel Res. Int.*, 2020, 92: 2000432.

[68] E.T. Turkdogan, Physical Chemistry of High Temperature Technology, Academic Press, New York, 1980.

[69] UNDESA, UN Sustainable Development Goals. Available from: https://sdgs.un.org/goals/goal9#targets_and_indicators [accessed 2024-02-20].

[70] UNDESA, UN Sustainable Development Goals. Available from: https://sdgs.un.org/goals/goal12#targets_and_indicators [accessed 2024-02-20].

